JACS
JOURNAL OF THE AMERICAN CHEMICAL SOCIETY
pubs.acs.org/JACS
Article

N-Heterocyclic Carbene to Actinide d-Based π-bonding Correlates with Observed Metal–Carbene Bond Length Shortening Versus Lanthanide Congeners

Conrad A. P. Goodwin, Ralph W. Adams, Andrew J. Gaunt,* Susan K. Hanson, Michael T. Janicke, Nikolas Kaltsoyannis,* Stephen T. Liddle, Iain May, Jeffrey L. Miller, Brian L. Scott, John A. Seed, and George F. S. Whitehead

Cite This: J. Am. Chem. Soc. 2024, 146, 10367–10380

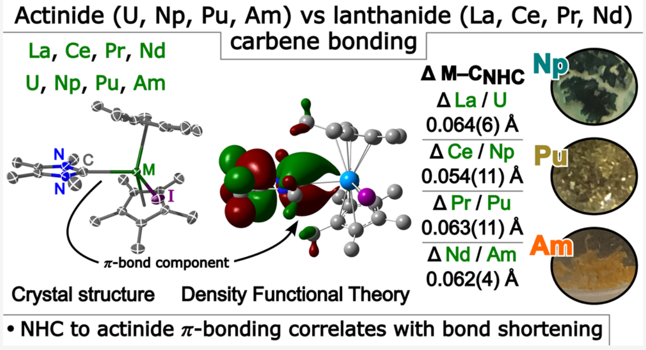

ABSTRACT: Comparison of bonding and electronic structural features between trivalent lanthanide (Ln) and actinide (An) complexes across homologous series' of molecules can provide insights into subtle and overt periodic trends. Of keen interest and debate is the extent to which the valence f- and d-orbitals of trivalent Ln/An ions engage in covalent interactions with different ligand donor functionalities and, crucially, how bonding differences change as both the Ln and An series are traversed. Synthesis and characterization (SC-XRD, NMR, UV–vis–NIR, and computational modeling) of the homologous lanthanide and actinide N-heterocyclic carbene (NHC) complexes $[M(C_5Me_5)_2(X)(I^{Me4})]$ {X = I, M = La, Ce, Pr, Nd, U, Np, Pu; X = Cl, M = Nd; X = I/Cl, M = Nd, Am; and $I^{Me4} = [C(NMeCMe)_2]$} reveals consistently shorter An–C vs Ln–C distances that do not substantially converge upon reaching Am^{3+}/Nd^{3+} comparison. Specifically, the difference of 0.064(6) Å observed in the La/U pair is comparable to the 0.062(4) Å difference observed in the Nd/Am pair. Computational analyses suggest that the cause of this unusual observation is rooted in the presence of π-bonding with the valence d-orbital manifold in actinide complexes that is not present in the lanthanide congeners. This is in contrast to other documented cases of shorter An–ligand vs Ln–ligand distances, which are often attributed to increased 5f vs 4f radial diffusivity leading to differences in 4f and 5f orbital bonding involvement. Moreover, in these traditional observations, as the 5f series is traversed, the 5f manifold contracts such that by americium structural studies often find no statistically significant Am^{3+}vs Nd^{3+} metal–ligand bond length differences.

■ INTRODUCTION

Our understanding of the chemical bonding and coordination chemistry of the lanthanide (Ln) and actinide (An) elements has evolved substantially over the last century.[1−7] Through this period, the postulate that Ln^{3+} cations operate in a highly ionic bonding regime, comparable to that of alkaline earth metals, has remained essentially unchanged.[3] The core-like 4f manifold is too radially contracted to engage in substantial spatial-overlap-driven covalent interactions with bound ligands. In contrast to the lanthanides, many actinides have multiple readily accessible oxidation states, and the greater radial expansion of the 5f manifold (versus 4f) can result in appreciable interaction with ligand orbitals,[8] though this decreases across the 5f row as Z_{eff} increases.[9−20] Complexes in higher oxidation states (e.g., IV–VI), particularly those of uranium which are more studied than transuranium complexes, frequently show that the more radially diffuse 6d manifold (versus 5f) is capable of accepting ligand density and participates in multiple bonding interactions such as in actinyl or mono-oxo ($\{AnO_x\}^{n+}$) or bis-($\{An(NR)_2\}^{n+}$) linkages,[21−24] and in other An=E combinations.[7,25−33] In some instances, the covalency of An=element multiple bonds, featuring rich 5f, 6d, and 7p components, can approach or surpass that of transition metal complexes.[34]

Differences between lanthanide and actinide complexes, brought about, at least in part, by variations in metal–ligand interactions, are exploited in separations science applications.[35−41] However, crystallographic studies comparing soft and hard σ-donor binding in metal pairs with similar ionic radii

Received: November 13, 2023
Revised: February 23, 2024
Accepted: February 26, 2024
Published: April 3, 2024

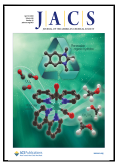

https://doi.org/10.1021/jacs.3c12721

(e.g., 6-coordinate Ce^{3+} = 1.01 Å; U^{3+} = 1.025 Å) often show that for hard (e.g., N, O) σ donors, the two metals behave similarly and display minimal bond length differences. In studies of soft donors (e.g., Se, Te, and N-heterocycles) with f-block metals, bonding differences are often observed between the lanthanide and actinide series; however, to the best of our knowledge,[11,14−18,20,42−47] in every homologous series studied thus far by single-crystal X-ray diffraction (SC-XRD), the magnitude of differences decreases to statistical insignificance as the f-block is traversed. This effect is such that by Am, an element challenging to separate/chemically distinguish from lanthanides, Am−ligand versus lanthanide−ligand bond length differences are usually statistically insignificant, at least with conventional statistical treatments.[48] Nevertheless, these differences are exploited in Am^{3+}, Cm^{3+}, and Ln^{3+} separation schemes.[36−41] Turning to π-bonding, where both metals are trivalent, Ln^{3+} ions are much less likely to have (energetically and spatially) accessible orbitals to engage in such interactions than An^{3+} ions.[49] With π-acids (e.g., CO, $\{CN\}^-$), actinide−ligand bonds are almost invariably shorter than lanthanide−ligand bonds,[50,51] but much more frequently, the corresponding lanthanide complexes are simply not isolable.[52−54] The prospect of U^{3+} 5f → L [or involving ligand symmetry-matched orbitals from the ($U^{3+}L_3$) fragment] π back-bonding has been advanced as a plausible mechanism to explain some of these differences.[52,55−61] The opposite case, of L → M π-bonding, is rarely documented outside of multiply bonded species, which are challenging to isolate for trivalent lanthanides, hindering comparative studies. In the case of amido and alkoxide systems which may permit L → M π-donation, reports show that where present this involves donation to the 5f manifold.[62,63] In some simple systems such as the $[MCl_6]^{3-}$ series, differences attributable to L → An π (L → 6d and 5f) contributions have been described.[64]

Furthermore, if π back-bonding from metal f orbitals drives an observable effect, then transuranium actinides might be expected to show a weaker effect than uranium due to radial contraction from larger Z_{eff}; thus, a homologous series that spans several trivalent actinides is necessary to establish the nature of π-bonding and how it changes as the 5f row is traversed—few such homologous series are well studied.[11,14−18,20,43−47,50,65−71]

NHCs (NHC = N-heterocyclic carbene) are classically regarded as strong C_{NHC} → M σ^2 donors which means they will bind tightly and form isolable complexes offering a promising avenue to address some of the hindering factors above. Indeed, some transuranium NHC-complexes have recently been reported.[25] Where orbital occupancy and overlap allow, synergic M → NHC π back-donation from low-valent transition metals is often observed (Figure 1 left). For Ln^{3+}, the valence electrons, where present, reside in highly spatially contracted 4f-orbitals and so M → NHC back-donation is likely to be weak or absent. The greater radial extent of the 5f valence orbital set on An^{3+} (relative to 4f) may be significant enough to drive observable physical differences, such as bond length differences, derived from the differing f-orbital properties.[51,56] Furthermore, many NHCs show nonzero $2p_z$ density at the carbenic carbon, which in principle can give rise to C_{NHC} → M π-bonding interactions − i.e., $\sigma^2\pi^x$ bonds, where x is small but nonzero (Figure 1 right).[72−80] The somewhat (relative to 4f) radially expanded 5f and 6d (vacant) orbital sets on An^{3+} ions could both provide spatial overlap to form C_{NHC} → M π-bonding interactions. As such, f-block NHC complexes present a potential testbed for the investigation of lanthanide/actinide structural differences derived from both f-based M → L π back-bonding and L → M f- or d-based π-bonding.

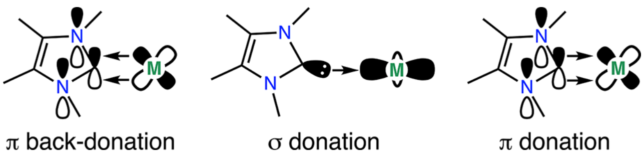

Figure 1. Various bonding interactions between an NHC ligand and d-orbitals.

Ephritikhine and co-workers have explored the binding of the simple NHC $\{C(NMeCMe)_2\}$, denoted I^{Me4} henceforth, to both Ce^{3+} and U^{3+} within the $[M(Cp^t)_3(I^{Me4})]$ (Cp^t = $\{C_5H_4$-*t*Bu$\}$) and also $[M(Cp^*)_2(I)(I^{Me4})]$ (Cp^* = $\{C_5Me_5\}$) frameworks.[51] High-quality single-crystal X-ray diffraction data were obtained from reactions using just $\sim$25-35 mg of starting material, and the data showed that the U−C_{NHC} distance was 0.037 Å shorter than Ce−C_{NHC}; note that (6-coordinate) Ce^{3+} is ca. 0.02 Å smaller than U^{3+}, which hinders an ideal comparison. Here, we report the preparation of $[M(C_5Me_5)_2(X)(I^{Me4})]$ (X = I, M = La, Ce, Pr, Nd, U, Np, Pu; X = Cl, M = Nd; X = I/Cl, M = Nd, Am) complexes which show unusually large differences in the M−C_{NHC} bond length between members of the trivalent lanthanide and actinide series with similar ionic radii, and those differences do not significantly reduce as the f-block series is traversed to include Nd^{3+}/Am^{3+} complexes.

RESULTS AND DISCUSSION

Synthesis of $[M(Cp^*)_2(I)(THF)]$ Complexes. Lanthanide $[Ln(Cp^*)_2(I)(THF)]$ (**1M**, M = La, Ce, Pr, and Nd) complexes were synthesized on a ca. 150 μmol scale in an argon-filled inert-atmosphere glovebox at room temperature. THF was added to a solid mixture of binary MI_3 and a slight excess (2.2 equiv) of KCp* in a glass scintillation vial with a Teflon-coated stirrer bar (Scheme 1). Workup and crystallization from warm toluene with a drop of THF (12 mg) gave free-flowing plank-shaped crystals of each complex in poor to fair yield (ca. 30−50%), though the exact % yields depend upon the amount of coordinated THF in each batch of "$M(Cp^*)_2(I)(THF)_m$" (M = La, Ce, Pr, Nd; *m* = 0 to 1) which remained after drying (see Supporting Information). The corresponding actinide complexes **1Np** and **1Pu** were synthesized using the previously reported procedure, beginning with $[AnI_3(THF)_4]$ (An = Np, Pu),[68] and were used as crude

Scheme 1. Synthesis of Isolated Crystalline $[M(Cp^*)_2(I)(THF)]$ (1M, M = La, Ce, Pr, Nd, Np, and Pu) from Trivalent Iodide Precursors

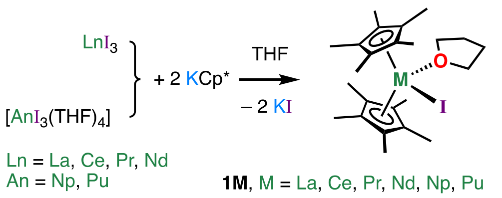

Scheme 2. Synthesis of Isolated Crystalline $[M(Cp^*)_2(I)(I^{Me4})]$ (2M, M = La, Ce, Pr, Nd, Y, Np, and Pu) from 1M, $[M(Cp^*)_2(I)(THF)]$, Prepared in Situ[a]

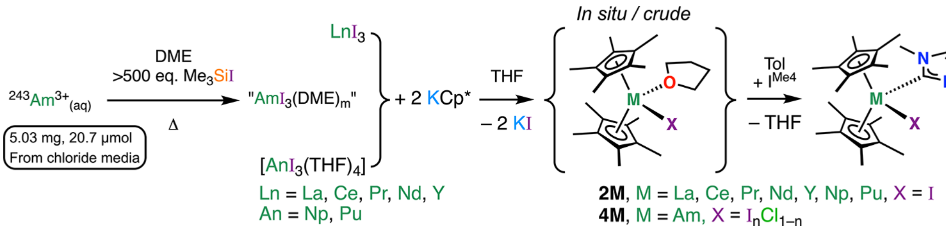

[a] I^{Me4} = $\{C(NMeCMe)_2\}$. Note that for M = Am, the X-atom depicted is a mixture of iodide and chloride.

products without recrystallization for subsequent reaction steps.

Synthesis of $[M(Cp^*)_2(I)(I^{Me4})]$ Complexes. Due to the poor solubility and stability of **1M** (M = La, Ce, Pr, Nd, Np, and Pu) in noncoordinating solvents such as toluene and hexane, we opted to synthesize all $[M(Cp^*)_2(I)(I^{Me4})]$ complexes (**2M**, M = La, Ce, Pr, Nd, Y, Np, Pu, and Am) from **1M** prepared in situ/as crude material (Scheme 2). A slight excess of solid I^{Me4} (1.05 equiv) was added to the stirred solutions of **1M** in toluene. Workup and low-temperature (−35 °C) crystallization from the reaction solvent gave **2M** in modest yield (30−40%) as well-isolated large plank-shaped crystals in all cases. We have included the yttrium compound, **2Y**, here as a smaller member of the series for comparative purposes, but the isolation of both **1Y** and **1Am** was not attempted (vide infra).

Rare earth **2M** compounds (M = La, Ce, Pr, Nd, and Y) were assessed by elemental analysis and found to be analytically pure and in agreement with their $[M(Cp^*)_2(I)(I^{Me4})]$ formulation. In the case of **2M** for Np and Pu, we can only judge their purity by ^1H and $^{13}C\{^1H\}$ NMR spectroscopies (vide infra). For the synthesis of **2Am**, we attempted to generate putative "$AmI_3(DME)_m$" in analogy to our previous synthesis of the chloride congener (Scheme 2).[14,81] The putative "$AmI_3(DME)_m$" was used as-synthesized for subsequent reaction steps—see Supporting Information for details. Instead of the anticipated Am^{3+} analogue of the other **2M** complexes, we isolated golden orange plank-shaped crystals of $[Am(Cp^*)_2(I_nCl_{1-n})(I^{Me4})]$ (**4Am**), where n is approximately 0.65 as determined independently by both ^1H NMR spectroscopy and single-crystal X-ray diffraction (vide infra). This suggests that the treatment of the putative "$AmCl_3(DME)_m$" precursor with $Me_3Si{-}I$ did not result in complete substitution of Cl for I. The corresponding Nd^{3+} complex $[Nd(Cp^*)_2(I_nCl_{1-n})(I^{Me4})]$ (**4Nd**, where n is also approximately 0.65) was then synthesized analogously starting from Nd^{3+} in aqueous 6 M HCl solution. Finally, to aid the interpretation of the bonding data in these mixed I/Cl **4M** complexes, $[Nd(Cp^*)_2(Cl)(I^{Me4})]$ (**5Nd**) was synthesized in low yield (24%) over two steps using binary $NdCl_3$ as the metal source.

Molecular Structures. Single-crystal X-ray diffraction studies revealed all four new **1M** complexes to be isomorphous to the previously reported **1U**, **1Np**, and **1Pu** (except **1La** for which the a axis is doubled in length), and the Sm,[82] Dy,[83] and Yb analogues.[84] All crystallize in the triclinic space group $P\bar{1}$ with two molecules per asymmetric unit ($Z' = 2$, except **1La** for which $Z' = 4$)—the structure of **1Ce** is depicted in Figure 2. Detailed discussion of structural metrics for **1M** is provided in the Supporting Information and is summarized in Tables 1 & 2 and Figure 4 to facilitate ready comparison to **2M** complexes (vide infra).

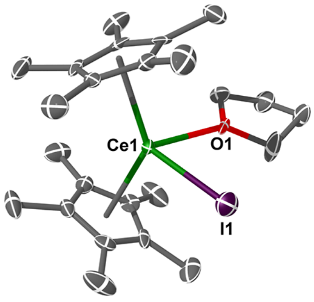

Figure 2. Molecular structure of **1Ce**. Ellipsoids set at 50% probability and H atoms, along with a second unit containing Ce(2), removed for clarity (operations: X, Y, Z). Ce(1)−I(1) = 3.1027(8) Å; Ce(1)−O(1) = 2.511(5) Å; Ce(1)−Cp_{cent} = 2.497(5) Å; Ce(1)−Cp_{cent} = 2.506(4) Å; Cp_{cent}−Ce−Cp_{cent} = 136.04(11)°.

The NHC-ligated complexes **2M** (M = La, Ce, Pr, Nd, Y, Np, and Pu) and $[M(Cp^*)_2(I_xCl_{1-x})(I^{Me4})]$ (M = Nd, **4Nd**; Am, **4Am**) isolated herein are isomorphous with the previously reported **2U** and **2Ce** analogues,[51] crystallizing in the monoclinic space group $P2_1/c$ with one molecule per asymmetric unit. In the case of **2La** and **2Ce** an additional polymorph was identified (see Supporting Information Tables S14 and S15 for more details). The structures of **2Pu** and **4Am** are shown in Figure 3. These complexes display a pseudo-tetrahedral bent-metallocene structure with a staggered Cp*···Cp* arrangement, like **1M**, as would be expected for a simple replacement of the THF moiety with the I^{Me4} NHC. Crystallographically characterized Pu−NHC complexes, and Pu−C σ-bonds in general, remain extremely scarce;[50,67,69,85] also, to the best of our knowledge, **4Am** represents the first structural authentication of an Am−C σ-bonding interaction to any organic ligand.

To investigate the influence of the mixed Cl/I occupancy in **4Am** on the overall structure, the Nd-congener, **4Nd**, was structurally characterized as well as the pure chloride Nd-analogue, $[Nd(Cp^*)_2(Cl)(I^{Me4})]$ (**5Nd**). The Cp_{cent}−M−Cp_{cent} angles for all **2M** lie over an exceptionally narrow range of ca. 135.20(8)−135.89(6)° (135.61(9)° using the mean and a weighted standard deviation as the error).[48] The M−Cp_{cent} ranges in **2M** [e.g., 2.5576(17)−2.5708(15) Å for **2La** and 2.4941(13)−2.5081(12) Å for **2Nd**] are nevertheless very close and on the order of only ca. 0.03 Å longer than **1M**, while statistically distinct from those in the corresponding **1M** complexes. The Cp_{cent}−M−Cp_{cent} angles for **4Nd** (135.18(11)°) and **4Am** (135.64(6)°) are very close or actually overlap with the average for all others (including **2Y**) at 135.61(9)°.[48,51] Similarly, both display M−C_{Cp} ranges

Table 1. Bond Lengths (Å) and Angles (deg) for M(1) in 1M (M = La, Ce, Pr, Nd, U, Np, and Pu)[a]

	1La[b]	1U[66]	1Ce	1Np[68]	1Pr	1Pu[68]	1Nd
M–I	3.1400(6)	3.0636(6)	3.1027(8)	3.0560(14)	3.0851(8)	3.0353(7)	3.0618(10)
M–O	2.536(4)	2.496(4)	2.511(5)	2.504(13)	2.491(5)	2.460(5)	2.461(8)
M–Cp$_{\text{cent}}$	2.562(4)	2.476(4)	2.497(5)	2.530(5)	2.473(5)	2.455(6)	2.467(6)
	2.542(16)	2.494(4)	2.521(4)	2.561(5)	2.500(5)	2.463(5)	2.471(7)
Cp$_{\text{cent}}$–M–Cp$_{\text{cent}}$	138.08(17)	135.56(9)	136.04(11)	135.12(11)	135.92(12)	135.49(13)	135.48(16)

[a] Due to different numbering conventions across some examples, "M(1)" is denoted here as that with the shortest M–I distance, and numbering proceeds from there. Except for **1La**, all are isomorphous. However, **1La** is isostructural. [b] Only the largest component of the disordered La–Cp rings is listed.

Table 2. Comparison of M–I and M–O Bond Lengths (Å) between 1M (M = La, Ce, Pr, U, Np, and Pu) Complexes

	M–I		M–O	
	M(1)	M(2)	M(1)	M(2)
1La	3.1400(6)	3.1492(5)	2.536(4)	2.531(4)
1U	3.0636(6)	3.0955(6)	2.496(4)	2.486(4)
Δ(La–U)	*0.0764(8)*	*0.0537(8)*	*0.040(6)*	*0.045(6)*
1Ce	3.1027(8)	3.1272(7)	2.511(5)	2.507(4)
1Np	3.0560(14)	3.0832(12)	2.504(13)	2.472(12)
Δ(Ce–Np)	*0.0467(8)*	*0.0440(7)*	*0.007(6)*	*0.035(6)*
1Pr	3.0851(8)	3.1070(8)	2.491(5)	2.499(5)
1Pu	3.0353(7)	3.0594(6)	2.460(5)	2.463(6)
Δ(Pr–Pu)	*0.0498(1)*	*0.0476(1)*	*0.031(6)*	*0.036(6)*
Δ(Ce–Pu)	*0.0674(11)*	*0.0678(9)*	*0.051(7)*	*0.044(7)*

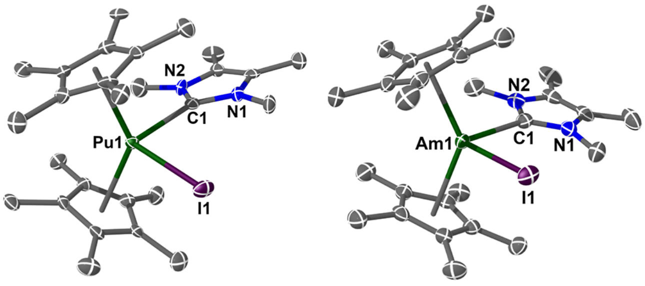

Figure 3. Molecular structure of **2Pu** and **4Am**. Ellipsoids set at 50% probability and H atoms removed for clarity (operations: *X*, *Y*, *Z*). In **4Am**, Cl(1) has been removed for clarity and the I(1) occupancy (0.65) has been refined competitively against Cl(1) (0.35). Pu(1)–I(1) = 3.0938(7) Å; Pu(1)–C(1) = 2.637(8) Å; Pu(1)–Cp$_{\text{cent}}$ = 2.489(4) Å; Pu(1)–Cp$_{\text{cent}}$ = 2.510(4) Å; Cp$_{\text{cent}}$–Pu(1)–Cp$_{\text{cent}}$ = 135.47(13)°. Am(1)–I(1) = 3.0666(11) Å; Am(1)–C(1) = 2.631(3) Å; Am(1)–Cp$_{\text{cent}}$ = 2.4744(17) Å; Am(1)–Cp$_{\text{cent}}$ = 2.4895(15) Å; Am(1)–Cl(1) = 2.682(8) Å; and Cp$_{\text{cent}}$–Am–Cp$_{\text{cent}}$ = 135.64(6)°.

(**4Nd**, 2.741(7)–2.816(7) Å; **4Am** 2.718(3)–2.802(3) Å), which follow smoothly from the previous members of their respective series, where the small decrease in length is commensurate with the reduction in ionic radius. Tables 3 and 4 summarize pertinent lengths and angles within the **2M** series and **4Am**/**4Nd**; see the Supporting Information for a comparison of **2La** and **2Ce** to their polymorphs (**2La**$^{\beta}$ and **2Ce**$^{\beta}$).

Complex **5Nd** crystallized in the triclinic space group $P\bar{1}$ with $Z' = 2$, unlike both **2M** (M = La, Ce, Pr, Nd, Y, U, Np, and Pu) and **4M** (M = Nd, Am), which suggests that beyond a certain chloride occupancy the bulk lattice changes. However, all pertinent bond lengths and angles for **5Nd** (e.g., Nd–C$_{\text{Cp}}$ range = 2.723(3)–2.85(3) Å; Nd–C$_{\text{NHC}}$ = 2.708(3) Å; Cp$_{\text{cent}}$–Nd–Cp$_{\text{cent}}$ = 134.3(4)° and 136.91(8)°) are very similar to both **2Nd** and **4Nd**. Between **2Nd**, **4Nd**, and **5Nd**, all metrical parameters overlap within the 3σ criterion with the exception of the Nd–I lengths (3.1209(2) Å in **2Nd**, and 3.103(2) Å in **4Nd**). This suggested that at least for Nd, within this molecular framework, there is a minimal perturbation to the rest of the molecular structure due to the influence of iodide (**2Nd**) vs chloride (**5Nd**)—though packing forces differ. Importantly, across all three structures with Nd, the Nd–C$_{\text{NHC}}$ bond lengths are within 3σ of each other except for one of the Nd–C$_{\text{NHC}}$ distances in **5Nd** (there are two independent molecules in the asymmetric unit); **2Nd**, 2.693(3) Å; **4Nd**, 2.683(7) Å; and **5Nd**, 2.667(3) Å and 2.708(3) Å. Thus, we suggest that it is possible to draw useful comparisons with other mixed-halide structures such as **4Am**—noting that M–X (X = I or Cl) bond lengths are likely to be somewhat less reliable than those from a data set which does not contain mixed occupancy atoms.

The M–C$_{\text{NHC}}$ bond lengths within the **2M** series provide the most striking comparison. For example, with **2La** and **2U**,

Table 3. Experimental and (in Italics) Computed (Vide Infra) Bond Lengths (Å) and Angles (deg) for 2M (M = La, Ce, Pr, Nd, Y, U, Np, and Pu), and 4M (M = Nd, Am)

	2La	2U[51]	2Ce[a]	2Np	2Pr	2Pu	2Nd	4Nd	4Am	2Y
M–I	3.1769(3)	3.1266(4)	3.1584(6)	3.1003(7)	3.1393(6)	3.0938(7)	3.1209(2)	3.103(2)	3.0666(11)	3.0409(4)
	3.140	*3.095*	*3.118*	*3.081*	*3.100*	*3.074*	*3.085*	–[b]	–[b]	
M–C$_{\text{NHC}}$	2.751(4)	2.687(5)	2.724(7)	2.670(9)	2.700(7)	2.637(8)	2.693(3)	2.683(7)	2.631(3)	2.583(4)
	2.754	*2.667*	*2.720*	*2.665*	*2.698*	*2.643*	*2.690*	–[b]	–[b]	
M–Cp$_{\text{cent}}$	2.5590(17)	2.514(3)	2.534(4)	2.495(4)	2.511(3)	2.489(4)	2.4941(13)	2.500(4)	2.4744(17)	2.3967(15)
	2.5723(15)	2.532(2)	2.547(3)	2.518(4)	2.529(3)	2.510(4)	2.5081(12)	2.511(3)	2.4895(15)	2.4126(15)
Cp$_{\text{cent}}$–M–Cp$_{\text{cent}}$	135.45(5)	135.20(8)	135.92(11)	134.82(14)	135.95(11)	135.47(13)	135.30(4)	135.18(11)	135.64(6)	135.89(6)

[a] **2Ce** has been reported previously;[51] however, we have resynthesized it here and used values from our single-crystal X-ray diffraction study. Mean absolute deviation between the experiment and calculation = 0.032 Å for M–I and 0.006 Å for M–C. [b] Geometry optimization was not performed on the **2Am** component of **4Am** due to the unavailability of dispersion corrections for Am,[86] and the **2Nd** component of **4Nd** was not optimized as **2Nd** has been geometry-optimized separately starting from coordinates from crystals of the pure compound.

Table 4. Comparison of Experimental and Computed M−I and M−C_{NHC} Bond Lengths (Å) between 2M (M = La, Ce, Pr, U, Np, and Pu) and 4M (M = Nd, Am) Complexes

	M−I		M−C_{NHC}	
	Expt.	Comp.	Expt.	Comp.
2La	3.1769(3)	3.140	2.751(4)	2.754
2U	3.1266(4)	3.095	2.687(5)	2.667
Δ(La−U)	*0.0503(5)*	*0.045*	*0.064(6)*	*0.087*
2Ce	3.1584(6)	3.118	2.724(7)	2.720
2Np	3.1003(7)	3.081	2.670(9)	2.665
Δ(Ce−Np)	*0.0581(9)*	*0.037*	*0.054(11)*	*0.055*
2Pr	3.1393(6)	3.100	2.700(7)	2.698
2Pu	3.0938(7)	3.074	2.637(8)	2.643
Δ(Pr−Pu)	*0.0455(9)*	*0.026*	*0.063(11)*	*0.055*
Δ(Ce−Pu)	*0.0646(9)*	*0.044*	*0.087(11)*	*0.077*
2Nd	3.1209(2)	3.085	2.693(3)	2.690
4Am	3.0666(11)	–[b]	2.631(3)	–[b]
Δ(Nd−Am)[a]	*0.0543(11)*	–[b]	*0.062(4)*	–[b]
4Nd	3.103(2)	–[b]	2.683(7)	–[b]
Δ(Nd−Am)[a]	*0.0364(20)*	–[b]	*0.052(8)*	–[b]

[a] Entries compare **4Am** to **2Nd**, or **4Nd**, respectively. [b] Geometry optimization was not performed on the **2Am** component of **4Am** due to the unavailability of dispersion corrections for Am,[86] and the **2Nd** component of **4Nd** was not optimized as **2Nd** has been geometry-optimized separately starting from coordinates from crystals of the pure compound.

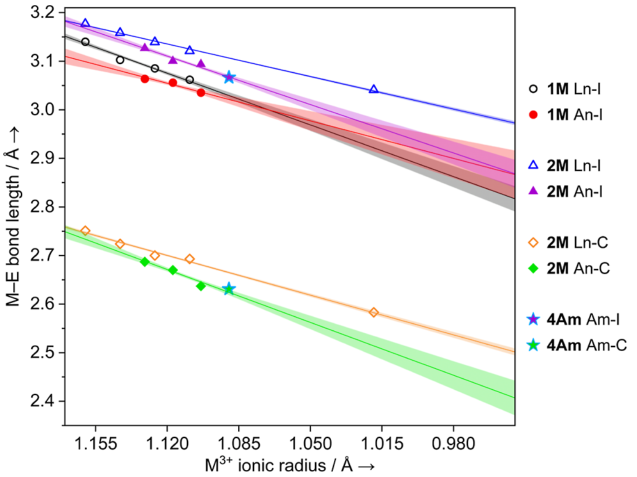

Figure 4. M^{3+} ionic radius (calculated 8-coordinate)[14] vs the M−E bond length for M−I with both **1M** and **2M**, and M−C_{NHC} for **2M** and **4Am**. Open symbols are used for Ln complexes (La, Ce, Pr, Nd, and Y from left to right), and solid symbols are used for An complexes (U, Np, Pu, and Am from left to right). Solid lines denote a linear fit of the data points (see Supporting Information for statistical parameters), and shaded areas show the 50% confidence interval for extrapolated data. For the **1M** series, only metal site (1) is shown here, which corresponds in all cases to the shorter M−I length, to minimize the differences and not overstate any conclusions. See Supporting Information for additional data plots.

the difference in the M−C_{NHC} bond (Δ = 0.064(6) Å) is similar to the difference between **2Pu** (M−C_{NHC} = 2.637(8) Å) and either **2Ce** (M−C_{NHC} = 2.724(7) Å; Δ = 0.087(11) Å) or **2Pr** (M−C_{NHC} = 2.700(7) Å; Δ = 0.063(11) Å). Crucially, the difference in M−C_{NHC} lengths between the lanthanide and actinide series does not diminish significantly from U to Pu (La to Pr). By comparison, as Tables 2 and 3 show, the magnitude of the difference between lanthanide and actinide M−I bond lengths broadly decreases along both **1M** and **2M** series, which is the normal trend.[18,20,47,65,87−90] In **4Am,** we see that the M−C_{NHC} length (2.631(3) Å) is shorter than all of the **2M** (M = La, Ce, Pr, Nd, U, Np, and Pu) complexes except that of **2Y**. When comparing **4Am** to all of **4Nd**, **2Nd**, and **5Nd** (8-coordinate ionic radii: Am^{3+} = 1.09 Å, Nd^{3+} = 1.109 Å; Δ = 0.019 Å), we find that none of the Nd-complexes has any overlap of their Nd−C_{NHC} lengths with the Am−C_{NHC} bond in **4Am**, even to a 5σ level of significance. For example, the difference in the M−C_{NHC} bond between **4Am** and **2Nd** is 0.062(3) Å (with **2Nd** bearing the longer bond length), and for **4Nd,** it is 0.082(8) Å, again where Nd bears the longer distance. The smallest difference between **4Am** and any of the Nd^{3+} complexes we observe is when comparing Nd(1) of **5Nd** with **4Am** (Δ = 0.036(4) Å)—again this difference is larger than the difference in their ionic radii even when accounting for the standard uncertainty in the measurements. To the best of our knowledge, this is unprecedented in studies of molecular systems with trivalent f-elements that span across La/U, Ce/Np, Pr/Pu, and Nd/Am comparisons. Figure 4 shows a plot of the calculated 8-coordinate ionic radius vs the M−E bond length for M−I in **1M**, and both M−I and M−C_{NHC} in **2M**.[14,91] See Figure S44 in the Supporting Information for the same data plotted against the experimentally derived 6-coordinate ionic radii, which shows the same trend.

In assigning the coordination numbers of complexes herein, we have counted Cp as three sites;[92] therefore, the metals are formally 8-coordinate, and so values for 8-coordinate ionic radii are used.[14,91] This is to avoid overstating the significance of bond length differences, which can manifest when 6-coordinate radii are used with complexes which are not formally 6-coordinate. When comparing isomorphous Am and Nd complexes with formal coordination numbers (CN) greater than 6—which is every molecular Am complex to have been structurally characterized except $[Am\{N(O{=}PPh_2)_2\}_3]$ (6 CN),[14] $[AmBr_3(OPCy_3)_3]$ (6 CN),[89] and $[AmCl_6][PPh_4]_3$ (6 CN)[64] – one should account for the 0.019 Å difference between 8-coordinate Am^{3+} and Nd^{3+}. When Am-ligand bond lengths are shorter than Nd-ligand bond lengths by >0.019 Å, they are more likely to be of significance beyond simple well-established ionic bonding trends as opposed to shortening, which lies between 0.008 and 0.019 Å.

It is important to place the metrical data in context with previous Am/Nd comparisons in the literature, which reflects the scarcity of clear, unambiguous cases where Am^{3+}-ligand bond lengths are shorter than Nd^{3+}-ligand bond lengths. By way of example, the M−Se bond lengths in a series of 9-coordinate complexes, $[M\{N(E{=}PPh_2)_2\}_3]$ (M = La, Ce, Nd, U, Np, Pu, and Am; E = Se),[14,68] show that the An−Se length is shorter than the Ln−Se length for U/La and Pu/Ce pairs by 0.0360(5) and 0.0303(4) Å, but upon reaching Am/Nd, the difference dropped to 0.0176(9) Å which is on the edge of the difference in the 8-coordinate ionic radii of Am^{3+}/Nd^{3+} (Δ = 0.019 Å), while much larger than the difference in 6-coordinate ionic radii for these metals (Δ = 0.008 Å)—noting of course that these complexes are 9-coordinate.[91] In $[M(Cp^{tet})_3]$ [M = Am, Nd; Cp^{tet} = (C_5Me_4H)], the Am−$Cp_{centroid}$ distance is 2.517(8) Å and 2.518(1) Å for the Nd−$Cp_{centroid}$ distance, meaning that they are statistically identical.[81] In $[\{M(Cp')_3\}_2(\mu\text{-}4,4'\text{-bipy})]$ (M = Am, Nd; Cp′ = $\{C_5H_4(SiMe_3)\}$; bipy = bipyridine),[18] the average Am and Nd M−$Cp_{centroid}$ distances to the Cp′ ligand are 2.524(3) and

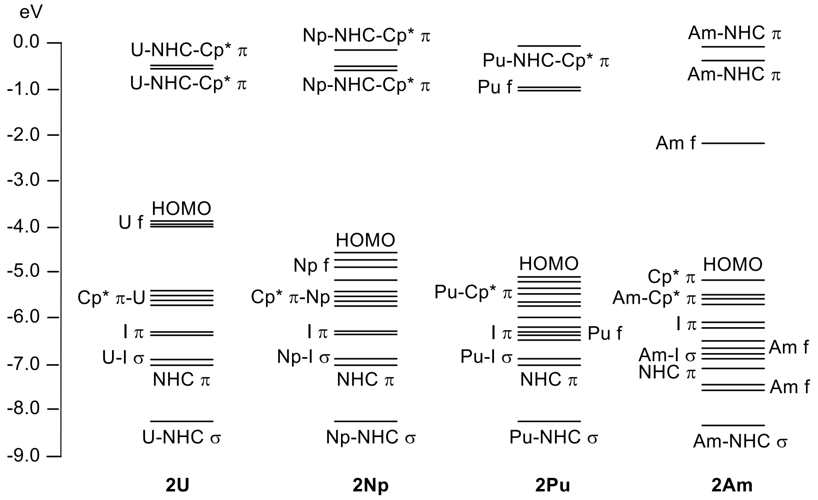

Figure 5. Molecular orbital energy level diagrams for **2An** (An = U, Np, Pu, and Am), obtained from the optimized geometries of **2U**, **2Np**, and **2Pu**, and from a single point calculation at the single-crystal X-ray diffraction geometry of the **2Am** component of **4Am** (due to unavailability of dispersion corrections for Am).[86] Principal orbital character is indicated, though sometimes the indicated character is present in other, energetically close, orbitals. HOMO = highest occupied molecular orbital.

2.543(2) Å, respectively, (Δ = 0.019(4) Å)—again on the edge of significance when the differences in 8-coordinate ionic radius is considered.[92] The difference in the metal−nitrogen distances is slightly more pronounced in the $[\{M(Cp')_3\}_2(\mu\text{-}4,4'\text{-bipy})]$ complexes, where the Am−N bond (2.618(3) Å) is shorter than the Nd−N bond (2.6482(16) Å) by 0.030(3) Å.[18] In a study of f-block dithiocarbamate complexes, $[M(S_2CNEt_2)_3(N_2C_{12}H_8)]$ (M = Nd, Sm, Eu, Gd, Dy, Am, Cm, and Cf), the average Am−N and Am−S distances were found to overlap within 3*σ* of each other once ionic radius differences were considered.[46] Similarly, inconclusive signs of Am vs Nd bonding differences were found in a pair of dithiophosphinate complexes, $[M\{S_2P({}^tBu_2C_{12}H_4)\}_4]^-$ (M = Am, Nd), which feature ligands directly relevant to S-donor extractant molecules that show selectivity for the minor actinide ions Am^{3+} and Cm^{3+}, over Ln^{3+}, in biphasic solvent extractions.[14,16,68,88] Thus, the substantially shorter $Am−C_{NHC}$ length in **4Am** compared with the isomorphous **4Nd** congener is unusual and warrants further spectroscopic/computational investigation to provide insight into the origin of the observed metrical differences.

Quantum Chemical Calculations. To help elucidate the nature of the bonding and electronic structure differences in complexes **2M**, we turned to computational quantum chemistry in the form of scalar relativistic, hybrid density functional theory at the PBE0 level. Full details of the calculations are given in the Supporting Information. We began by optimizing the geometries of **2M** (M = La, Ce, Pr, Nd, U, Np, and Pu); M−I and $M−C_{NHC}$ distances are collected in Tables 3 and 4. There is very good agreement in these metrics between experiment and calculation, especially for $M−C_{NHC}$ lengths, for which the mean absolute deviation is only 0.006 Å. As with the single-crystal X-ray diffraction data, the difference between the M−I distances in corresponding pairs of lanthanides and actinides decreases systematically across the series, while the analogous difference in $M−C_{NHC}$ distances does not, with that of the Pr/Pu pair being the same as that for Ce/Np, Δ = 0.055 Å. Note that due to the unavailability of dispersion corrections for Am,[86] the structure of **2Am** was not optimized and was taken directly from the single-crystal X-ray diffraction geometry (that is, the iodo-component of **4Am**).

We initially anticipated that natural bond orbital (NBO) analysis would allow us to address the nature of the $M−C_{NHC}$ interaction within a localized orbital framework, but NBO did not locate any $M−C_{NHC}$ bonding orbitals. Therefore, we turned to an analysis of the Kohn−Sham orbitals, recognizing that these are typically rather delocalized in large, low-symmetry f-element organometallic compounds. Valence molecular orbital (MO) energy level diagrams are presented for **2An** (An = U, Np, Pu, Am) in Figure 5, with analogous diagrams for **2Ln** given in the Supporting Information (Figure S96). The energies of the An−Cp* and An−I orbitals change little across the series, in contrast to the metal 5f manifold, which shows the expected significant decrease in energy from U to Am. The NHC-based MOs—distinguished as *σ* and *π* according to their principal character about the M···C axis—are the most stable of those shown, except for **2Am**, for which two metal 5f-based orbitals lie in between the NHC-based levels (also the case for **2Nd**, see Figure S96).

Before exploring the composition of the NHC-based *σ* and *π* MOs, it is instructive to examine the total energy surface for scanning the $M−C_{NHC}$ distance. Figure 6 shows the change in the total (SCF) energy of **2La** and **2U** upon performing relaxed scans of this distance. Clearly, these energy surfaces are very flat; compressing or elongating the bonds by 0.05 Å, an amount similar to the Ln vs An bond length differences seen in the **2M** series, costs only ca. 0.5 $kJ\cdot mol^{-1}$, suggesting that quantum chemical differences in $M−C_{NHC}$ bonding between Ln/An pairs are likely small. The energy penalties for the $M−C_{NHC}$ bond length changes are within the range of crystal packing forces, but the consistent shortening of $An−C_{NHC}$ relative to $Ln−C_{NHC}$ within this series, to a degree which is not commensurate with the difference in ionic radius, suggests that the crystal packing forces are not the main cause. It is notable that the energy well for **2U** is slightly steeper than that for **2La**, suggesting that the $U−C_{NHC}$ bond is the stronger. To further estimate this, we split both **2U** and **2La** into two fragments, the NHC ligand and the Cp_2^*MI component at their geometries in **2U** and **2La**, and calculated the energies of the separated

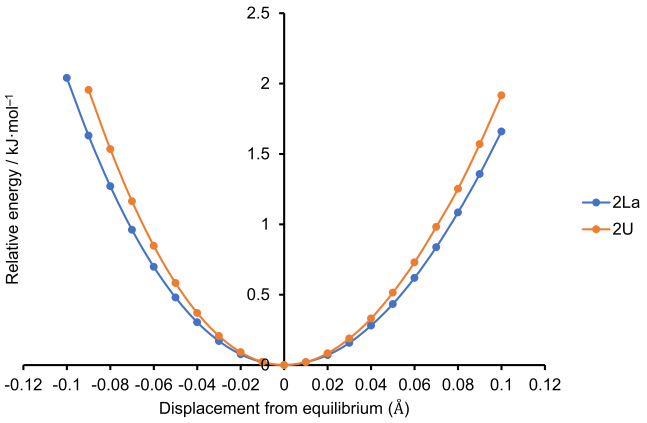

Figure 6. Energy relative to that at the fully optimized geometry for changing the M−C_{NHC} distance in **2La** and **2U**, while allowing the rest of the atomic positions to relax.

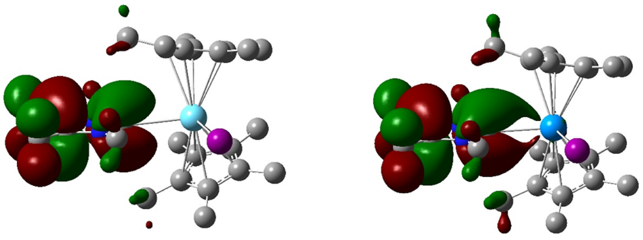

Figure 7. NHC-based π molecular orbital in **2La** (left) and **2U** (right), isovalue = 0.02. Hydrogen atoms omitted for clarity.

fragments vs those of the full molecules. This yields fragmentation energies of 192.6 and 174.4 kJ·mol^{-1} for **2U** and **2La**, respectively, at the SCF level.

Table 5 presents Mulliken population analysis data for the NHC-based σ and π MOs, together with the M−C delocalization indices δ, calculated from the quantum theory of atoms in molecules (QTAIM). δ is often taken as a QTAIM measure of bond order. None of the δ values are large, indicating that the M−C_{NHC} interactions are not strong, in agreement with Figure 6. The δ values display a striking similarity among the lanthanides, and within the actinide series. The latter have slightly higher δ than the former, suggestive of a consistently larger M−C_{NHC} interaction in the 5f series, in agreement with the experimental and computational structural data.

Turning to the population analysis of the NHC-based σ and π MOs, we begin with the former. It is noteworthy that, within the first three Ln/An pairs, the sum of the metal s, p, and d contributions to these orbitals is very similar, all lying within the range 10.3−11.0%. For the actinide member of each pair, there is also a 5f contribution, which rises from 1.4% for **2U** to 3.3% for **2Pu** (noting also the 1.4% 4f contribution for **2Pr**). **2Am** differs from the other actinides in having reduced s + p + d and larger 5f (6.7%) composition, though it has a total metal contribution very similar to **2Np** and **2Pu**. It is tempting to ascribe the shorter An−C_{NHC} distances vs their Ln analogues to the extra f content of the σ MO, but while recognizing that we cannot rule this out as a contributory factor, we sound the following cautionary note: Bursten's FEUDAL (f's essentially unaffected, d's accommodate ligands) model of the bonding in early actinide complexes tells us that, in general, it is the metals' d-orbitals that are primarily responsible for metal−ligand binding, not the 5f. Furthermore, it is well known that periodic increases in metal f contributions to MOs featuring both metal and ligand content typically arise from atomic orbital energy matching, rather than reflecting overlap-driven covalency. We note that the M−C_{NHC} distances in **2Pu** and **2Am** are almost identical, despite the Am 5f contribution to the σ MO being twice that in **2Pu**.

The structural data suggest that we are looking for a consistent difference in the An−C_{NHC} versus Ln−C_{NHC} bonding, a conclusion supported by the δ values in Table 5. Figure 6 tells us that such a difference is likely small, and the FEUDAL approach directs us to the 6d orbitals.[93−97] It is therefore noticeable that all of the actinide complexes have a very small but consistent metal d contribution to the NHC-based π MOs (Table 5), which is absent in all of the lanthanide systems. Complexes **2Pu** and **2Am** also have small 5f contributions to this MO, but note the arguments above about the nature of 5f-based covalency in this part of the actinide series. Figure 7 presents images of the NHC-based π MOs in **2La** and **2U**; the metal contribution to the latter is clearly visible.

If there is An−C_{NHC} bonding with a π-bonding component as described above, we would expect that rotating the NHC ligand about the M−C_{NHC} axis would be energetically more costly in the An vs Ln systems. We therefore attempted relaxed total energy surface scans for this distortion in **2La** and **2U**, but these calculations were not well-behaved, and indeed, the NMR spectroscopic data (vide infra) suggest that rotation about the M−NHC bond is a high-energy process, requiring significant structural rearrangement. Instead, Figure 8 presents the energies relative to that of the fully optimized geometry for

Table 5. Kohn−Sham Molecular Orbital Compositions (Mulliken Analysis, 1% Threshold) and QTAIM Delocalization Indices (δ) for 2M (M = La, Ce, Pr, Nd, U, Np, Pu, and Am)[a]

	2La	2U	2Ce	2Np	2Pr	2Pu	2Nd	2Am
metal content of M−NHC σ (%)	2.0s, 1.8p, 6.8d	1.9s, 1.0p, 7.7d, 1.4f (s + p + d = 10.6)	1.9s, 1.9p, 7.2d	1.8s, 1.1p, 7.4d, 2.4f (s + p + d = 10.3)	1.9s, 1.7p, 7.0d, 1.4f (s + p + d = 10.7)	1.8s, 1.2p, 7.4d, 3.3f (s + p + d = 10.6)	[b]	1.1s, 5.4d, 6.7f (s + p + d = 6.5)
total metal content (%)	10.6	12.0	11.0	12.7	12.1	13.8		13.2
metal content of M−NHC π (%)		1.3d		1.2d	[b]	1.2d, 3.4f		1.2d, 1.4f
M−C_{NHC} δ	0.30	0.38	0.31	0.38	0.31	0.38	0.31	0.37

[a]Data obtained from the optimized geometries of all **2M** bar **2Am**, for which a single point calculation at the single-crystal X-ray diffraction geometry was performed (due to non-availability of dispersion corrections for Am). [b]Extensive mixing of ligand orbitals with metal 4f levels (see Supporting Information Figure S96) precludes clear population analysis.

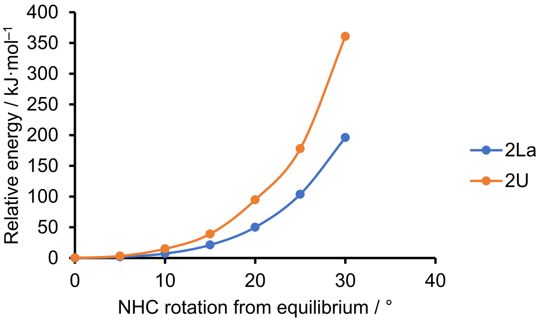

Figure 8. Energy relative to that at the fully optimized geometry for rotating the NHC ligand about the *M*−*C* axis in **2La** and **2U**, while keeping the rest of the atomic positions fixed.

rotating the NHC ligand while keeping all the other atomic positions fixed. Such an approach yields relative energies larger than in relaxed energy surface scans but typically provides an upper bound to the energetics. Clearly, from the ^{1}H NMR data of all **2M** complexes, there is a penalty for rotating the NHC ligand about the metal as evidenced by the inequivalence of the Me-resonances at room temperature. This is likely to be predominantly steric in origin as it is seen even for **2La**. However, computationally, the energy penalty for rotating the NHC ligand in **2U** is significantly larger than in **2La**. This may, in part, reflect the ca. 0.1 Å shorter U−C_{NHC} distance vs the La equivalent but may also result in part from the differing M−NHC orbital character shown in Figure 7.

QTAIM bond critical point (BCP) ellipticities ε can give information on single vs multiple bonding; values close to zero indicate cylindrical symmetry about the BCP (single or triple bonds), while significant deviations from zero suggest (partial) double bonding. In our experience, f-element−ligand BCP electron densities are typically very low, which can lead to highly variable curvatures (and hence curvature ratios, which define ε). The BCP electron densities ρ in our target systems are indeed small; those in **2Ln** range from 0.042 electron·bohr^{-3} (for **2La**) to 0.045 for **2Pr** and **2Nd**, with those for **2An** being slightly larger, at 0.051 for **2U**, rising to 0.052 for **2Pu** and **2Am**. Such low values do indeed lead to some scatter in the ε values, but, in general, these are larger for the actinide−NHC bonds than for the lanthanide analogues, the clearest separation being 0.261/0.023 for **2Np** vs **2Ce** and 0.283/0.091 for **2Pu** vs **2Pr**. Lastly, we note that during the revision stage of this manuscript, a report was published that documented a plutonium complex with a Pu−C_{NHC} interaction, complementing earlier analogous neptunium chemistry.[25,98] That research was focused on the characterization of Pu═C multiply bonded interactions through the coordination of diphosphonioalkylidene ({$C(PPh_2{=}NSiMe_3)_2$}, BIPM) ligands to the actinide metal ion. One of those complexes also contained coordinated I^{Me4} NHC ligands, for which shorter Np−C_{NHC} vs Ce−C_{NHC} and Pu−C_{NHC} vs Pr−C_{NHC} bonds were observed with differences on the order of ~0.045−0.060 Å. Consistent with this study, the bonding was found to be largely electrostatic in nature, but in those works, no differences in molecular orbital compositions related to the metal−NHC bonding were found to correlate with the bond metrics, nor were La/U and Nd/Am comparisons possible.

NMR Spectroscopy. To further support the characterization of the complexes herein, NMR spectra were collected for **1M** (M = La, Ce, Pr, Nd) in d_6-benzene with the addition of a weighed amount of H_8-THF to prevent precipitation of the insoluble material. We were able to observe the C_5Me_5 singlet for all four molecules by ^{1}H NMR (see Supporting Information for full details). Room temperature solution magnetic susceptibilities were determined for **1Ce**, **1Pr**, and **1Nd** by the Evans method, and they agreed well with the free-ion values: **1Ce** ($^2F_{5/2}$, measured: 2.47 μ_B vs 2.54 μ_B expected), **1Pr** ($^3H_4$, measured: 3.48 μ_B vs 3.58 μ_B expected), and **1Nd** ($^4I_{9/2}$, measured: 3.58 μ_B vs 3.62 μ_B expected).

Well-resolved ^{1}H and $^{13}C\{^1H\}$ NMR spectra were also collected all **2M** complexes (except previously reported **2U**), as well as **4Am**, in neat d_6-benzene (see Supporting Information for $^{13}C\{^1H\}$ NMR spectroscopy and all data). As previously observed with **2Ce** and **2U**,[51] all **2M** complexes showed that rotation about the M−C_{NHC} bond is restricted. A variable temperature NMR (VT-NMR) of **2La** showed that even at 100 °C in d_8-toluene, the La−C_{NHC} bond is restricted (Figures S57−S59). As La^{3+} is the largest ion studied herein and **2La** possesses the longest M−C_{NHC} bond length, the calculated barrier to rotation in this complex represents a lower bound for this series of complexes. Nevertheless, it is highly disfavored as $\Delta S^{\ddagger} = -11.6$ J·K^{-1} mol^{-1} (−61.8 J·K^{-1} mol^{-1} to 38.5 J·K^{-1} mol^{-1}) and $\Delta H^{\ddagger} = 92.3$ kJ·mol^{-1} (74.6 kJ·mol^{-1} to 110.0 kJ·mol^{-1}), where the values in brackets are the 95% confidence intervals. Presumably, the large barrier arises through a combination of predominantly steric effects, though, in the case of the actinide complexes, there may also be a contribution from the M−C_{NHC} π-bonding component which is supported by calculations (Figure 8). Table 6 shows the ^{1}H NMR chemical shifts for the Cp* and I^{Me4} ligands of all **2M** complexes.

The ^{1}H NMR spectrum of **4Am** in d_6-benzene shows features similar to all the **2M** complexes but with an apparent doubling of every signal (see Figures S64−S67). A variable temperature NMR spectroscopic (VT-NMR) study in d_6-benzene (Figure S66), across a small temperature range due to radiological safety considerations, revealed that up to 50 °C, the peaks did not coalesce, nor did their relative ratios change. We attribute the doubling to the presence of a mixed halide species, $[Am(Cp^*)_2(I_nCl_{1-n})(I^{Me4})]$, which informed and is in

Table 6. ^{1}**H NMR Chemical Shifts (ppm vs d_6-Benzene Residual) for 2M (M = La, Ce, Pr, Nd, Y, U, Np, and Pu). Spectra Were Recorded at Ambient Temperature (295−298 K)**

	2La	2U[a][51]	2Ce	2Np	2Pr	2Pu	2Nd	2Y
C_5Me_5	2.17	0.68	6.10	0.77	13.61	1.65	11.82	2.09
I^{Me4} $C(CH_3)$	1.21	−53.99	−23.68	0.18	−70.81	1.25	−33.77	1.21
	1.36	−46.82	−19.34	0.54	−47.13	1.25	−25.74	1.35
I^{Me4} $N(CH_3)$	2.99	−11.19	−3.52	2.64	−13.10	3.94	−5.43	2.91
	3.54	−10.49	−3.23	4.27	−10.59	4.98	−4.70	3.66

[a] **2U** was reported previously in d_8-THF.

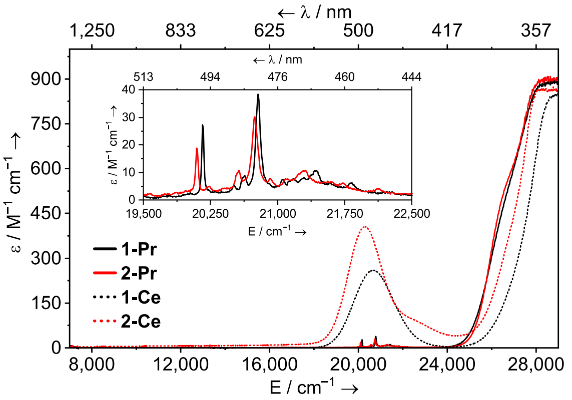

Figure 9. Solution UV−vis−NIR spectra of [M(Cp*)$_2$(I)(THF)] (**1M**, M = Ce, dotted black; Pr, solid black) (3 mM, THF) and [M(Cp*)$_2$(I)(I$^{\text{Me4}}$)] (**2M**, M = Ce, dotted red; Pr, solid red) (3 mM, toluene) shown between 7000 and 29,000 cm^{-1} (1429−345 nm) at ambient temperature.

excellent agreement with our crystallographic study (where *n* is ca. 0.65 determined by competitive refinement of the halide sites).

UV−Vis−NIR Spectroscopy. The UV−vis−NIR spectra of **1M** (M = La, Ce, Pr, and Nd) complexes were collected in THF at ambient temperature and can be compared with the spectra of their **2M** counterparts collected in toluene. Figure 9 shows the spectra of **1Pr**, **2Pr**, **1Ce**, and **2Ce** as examples. The influence of THF vs I$^{\text{Me4}}$ bonding on the f → f and f → d transitions in **1M** and **2M** is instructive toward the potential origin of the structural difference between the 4f and 5f series.

The absorption spectra of both **1Ce** and **2Ce** are simple and characteristic of Ce^{3+} (4f^1, $^2F_{5/2}$) complexes. A broad, somewhat featureless transition tails in from the UV region down to ca. 24,000 cm^{-1} (417 nm), and a single additional broad peak is observed, which is the 5d ← 4f dipole allowed interconfigurational transition. In **1Ce,** this is seen at 20,675 cm^{-1} (484 nm, ε = 259 M^{-1} cm^{-1}), and in **2Ce,** it lies at 20,308 cm^{-1} (492 nm, ε = 406 M^{-1} cm^{-1}), a red shift of 367 cm^{-1}. See the Supporting Information for a computational analysis of this transition, which supports this assignment. For Pr^{3+} (4f^2, $^3H_4$) ions, the 4f → 5d absorption energy is usually sufficiently large that it does not interfere with the vis−NIR absorption spectrum,[99−104] and it is the first member of the series for which f → f (Laporté forbidden, intraconfigurational) transitions are observed and thus can directly report on the impact of THF vs I$^{\text{Me4}}$ donor properties on the 4f manifold. The $^3P_0$ ← $^3H_4$ and $^3P_1$ ← $^3H_4$ transitions typically occur around 20,700 cm^{-1} (483 nm) and 21,400 cm^{-1} (467 nm), respectively.[99−101,103−105] In **1Pr** these appear at 20,161 cm^{-1} (496 nm, ε = 27 M^{-1} cm^{-1} for $^3P_0$) and 20,782 cm^{-1} (481 nm, ε = 38 M^{-1} cm^{-1} for $^3P_1$). In **2Pr**, these transitions occur at 20,097 cm^{-1} (498 nm, ε = 19 M^{-1} cm^{-1}) and 20,747 (482 nm, ε = 16 M^{-1} cm^{-1}), and so, like with **1Ce** and **2Ce** above, both exhibit a modest redshift in **2Pr** vs **1Pr**, though less than the cerium complexes. When comparing **1Nd** and **2Nd**, we see a much smaller redshift between most of the features than what is seen for the Ce^{3+} and Pr^{3+} complexes, though the spectra are much more complex (Figure S82), which precludes assigning a redshift value between any set of peaks. However, when comparing **2Nd** [Nd(Cp*)$_2$(I)(I$^{\text{Me4}}$)] to **5Nd** [Nd(Cp*)$_2$(Cl)(I$^{\text{Me4}}$)], we see essentially no difference (Figure S93) reflecting that replacing chloride with iodide has little impact upon the observed electronic transitions.

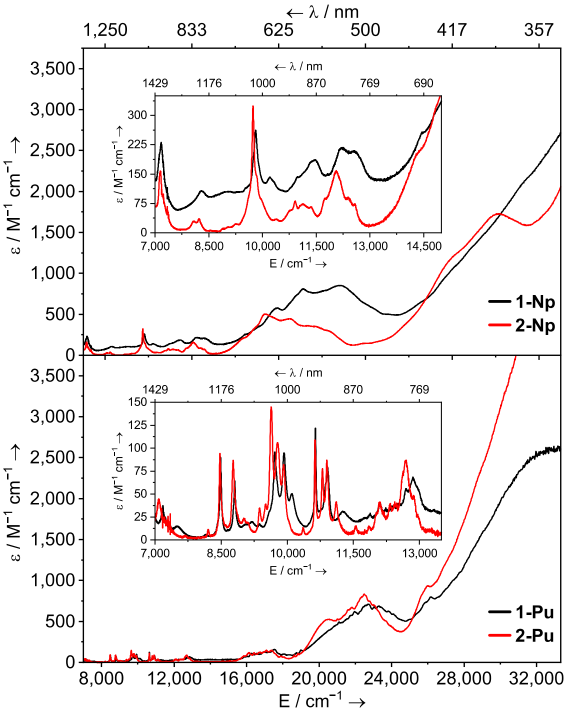

Figure 10. Top: solution UV−vis−NIR spectrum of [Np(Cp*)$_2$(I)(THF)] (**1Np**, black line) and [Np(Cp*)$_2$(I)(I$^{\text{Me4}}$)] (**2Np**, red line) in toluene. Bottom: solution UV−vis−NIR spectra of [Pu(Cp*)$_2$(I)(THF)] (**1Pu**, black line) and [Pu(Cp*)$_2$(I)(I$^{\text{Me4}}$)] (**2Pu**, red line). All spectra were collected in toluene at ambient temperature and are shown between 7000−33,333 cm^{-1} (1429−333 nm).

The UV−vis−NIR spectra of **2Np** and **2Pu** are remarkably similar to the previously reported spectra for **1Np** and **1Pu** (Figure 10).[68] All four feature broad absorptions which tail in from the UV region down to ca. 24,000 cm^{-1} (417 nm), which lead into a series of poorly resolved features presumably derived from the 6d ← 5f transitions with fine structure arising from splitting of the 5f manifold or vibronic coupling of the excited 6d state to ligand modes. For **1Np**, we previously noted a main band which extends from ca. 14,000−22,000 cm^{-1} (ca. 714−455 nm, ε_{max} = 849 M^{-1} cm^{-1}), which appears somewhat red-shifted in **2Np** and resides from ca. 13,000−20,000 cm^{-1} (769−500 nm, ε_{max} = 498 M^{-1} cm^{-1}; Figure 10 top). Complex **1Pu** shows a similar broad peak from ca. 18,000−25,000 cm^{-1} (556−400 nm, ε_{max} = 704 M^{-1} cm^{-1}), which appears much less red-shifted in **2Pu** (Figure 10 bottom) than between the Np^{3+} examples, such that the feature approximately overlaps the same range as in **1Pu** (i.e., 18,000−25,000 cm^{-1}; 556−400 nm; ε_{max} = 831 M^{-1} cm^{-1}). Fitting the peak groupings with a Gaussian curve (see Figures S94 and S95) shows the center of the main 5f → 6d grouping in **1Np** resides at 18,309(6) cm^{-1}, while for **2Np,** it is at 16,467(9) cm^{-1} which is roughly 1800 cm^{-1} lower in energy. For **1Pu** (22,947(7) cm^{-1}) and **2Pu** (22,211(13) cm^{-1}), the shift is much smaller at ca. 730 cm^{-1}. This trend of increasing energy in the 6d ← 5f transitions from Np to Pu is consistent with previous works.[68−70]

At the lower energy region of these spectra, characteristically weak and somewhat sharp Np^{3+} and Pu^{3+} f → f transitions can be seen[106−110] and are remarkably similar within each of the two pairs. As with **2Pr** and **2Nd**, there is a small red shift for

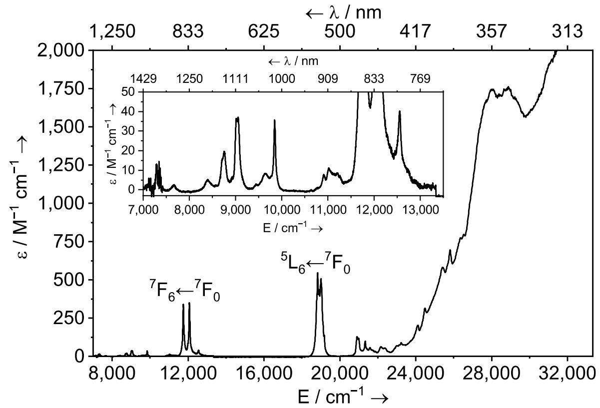

Figure 11. Solution UV−vis−NIR spectra of $[Am(Cp^*)_2(I_xCl_{1-x})(I^{Me4})]$ (**4Am**, ca. 1 mM, toluene) shown between 7000−33,000 cm^{-1} (1429−303 nm) at ambient temperature. Molar absorptivity values were based on using the MW of the mixed I/Cl species, but individual bands are not assigned to the specific I vs Cl species.

the I^{Me4} adduct vs the THF-adduct of ca. 70 to 200 cm^{-1} for **2Np**, depending on the pairs of peaks chosen, and at most ca. 150 cm^{-1} for **2Pu**.

Finally, the UV−vis−NIR spectrum of **4Am** (Figure 11) is broadly typical of Am^{3+} in solution, whereby we can identify features corresponding to the $^7F_6 \leftarrow {}^7F_0$ and $^5L_6 \leftarrow {}^7F_0$ transitions; however, both appear to be "doubled". In **4Am**, the higher-energy $^5L_6 \leftarrow {}^7F_0$ transition appears as two sharp peaks, 18,832 cm^{-1} (531 nm, ε = 544 M^{-1} cm^{-1}) and 19,004 cm^{-1} (526 nm, ε = 507 M^{-1} cm^{-1}), while the $^7F_6 \leftarrow {}^7F_0$ transition appears as two sharp peaks at 11,751 cm^{-1} (851 nm, ε = 340 M^{-1} cm^{-1}) and 12,071 cm^{-1} (828 nm, ε = 348 M^{-1} cm^{-1}). A similar, but genuine, splitting of the high energy $^5L_6 \leftarrow {}^7F_0$ feature was seen in $[Am(Cp^{tet})_3]$,[81] and also in $[\{Am(Cp')_3\}_2(\mu\text{-}4,4'\text{-bipy})]$.[18] With **4Am**, given the NMR and structural data which strongly suggest that the bulk is a mixture of $[Am(Cp^*)_2(I)(I^{Me4})]$ and the chloride congener, it is likely that the doubling is in fact due to differences in the f → f transitions of around 172 and 320 cm^{-1} for the major transitions in the iodide- and chloride-ligated complexes. This contrasts the little to no effect with Nd (vide supra).

The influence of THF vs I^{Me4} coordination on the f → f transitions in Np^{3+} and Pu^{3+} appears to be larger than seen with Pr^{3+} and Nd^{3+}, which might be expected based upon the better spatial overlap of the 5f orbitals with ligands vs that of the 4f orbitals in the lanthanide counterparts. However, it is smaller than the changes seen in the 5f → 6d region of all of the spectra, which suggests that the key differences in the way THF and I^{Me4} bind to these ions involve the 5d (lanthanide) and 6d (actinide) orbitals. These data support conclusions derived from the calculations.

CONCLUSIONS

Analysis across a series of NHC-ligated bent-metallocene complexes, $[M(Cp^*)_2(X)(I^{Me4})]$ (X = I, M = La, Ce, Pr, Nd, U, Np, and Pu; X = Cl, M = Nd; X = I/Cl, M = Nd, and Am), reveals significant shortening of the metal−C_{NHC} ligand bond length with actinide metals vs lanthanide examples with closely matched ionic radii. This homologous series extends from La to Nd and from U to Am, including rare or unique examples of M−C σ-bonding to NHC ligands in the case of Pu and Am. Most remarkably, we observe no significant decrease in the extent of An vs Ln metal−C_{NHC} length shortening as the series are traversed. Structural and quantum chemical analyses between the NHC complexes and their THF-ligated precursors reveal that hard/soft arguments of the primarily electrostatic origin explain the anticipated lanthanide vs actinide differences in M−I and M−O bond lengths. However, the An−NHC π-type Kohn−Sham molecular orbitals consistently feature small (ca. 1−2%) 6d contributions, which are absent for all the lanthanide congeners. Quantum theory of atoms in molecules data suggest a consistently larger M−C_{NHC} interaction in the 5f series, and the computed barrier to rotation of the NHC ligand around the U−C_{NHC} axis is larger than that for the La analogue. Together, these results suggest larger M−C_{NHC} covalency in the actinide series and that ligand-π to vacant 6d interactions can differentiate lanthanide and actinide ions with these neutral donor ligands. This is a key distinction between this molecular framework and others and could more generally inform the design of future ligand systems to differentiate otherwise similar f-block ions. Typically, lanthanide and actinide differences (within homologous donor series) are driven by the modest differences between the 4f and 5f manifold, but for the NHC complexes here, it is 6d orbital participation in the form of a minor π-bonding contribution in these simple Lewis-base adducts which is present in the actinide complexes but absent in the lanthanide congeners which correlates with substantial structural and spectroscopic differences. This bonding mechanism was proposed over 30 years ago with simple π-basic ligands on uranium, and this work presents evidence that extends deeper into the transuranium series.[94] In principle, strong σ-donor ligand systems capable of π-donation, such as amides or alkoxides, may show similar effects to those found herein. However, this may be restricted to metals in lower oxidation states (i.e., An^{3+}), as previous works on Np^{4+} alkoxides show π-donation into the 5f manifold, rather than 6d.[62] As organometallic chemistry of the transuranium elements is experiencing a renaissance as far across the actinide series as californium (the highest atomic number element which can be used for synthetic molecular chemistry on a mg scale), the results here suggest future studies into the role of d orbital-derived π-bonding beyond uranium, and indeed beyond americium, will be insightful.[71,111]

ASSOCIATED CONTENT

Supporting Information

The Supporting Information is available free of charge at https://pubs.acs.org/doi/10.1021/jacs.3c12721.

Experimental details, photographs taken during syntheses, crystallography details, molecular structure details and metrics, NMR and UV−vis−NIR spectra, and computational details (PDF)

Accession Codes

CCDC 2271531−2271546 contain the supplementary crystallographic data for this paper. These data can be obtained free of charge via www.ccdc.cam.ac.uk/data_request/cif, or by emailing data_request@ccdc.cam.ac.uk, or by contacting The Cambridge Crystallographic Data Centre, 12 Union Road, Cambridge CB2 1EZ, UK; fax: +44 1223 336033.

AUTHOR INFORMATION

Corresponding Authors

Andrew J. Gaunt − *Chemistry Division, Los Alamos National Laboratory, Los Alamos, New Mexico 87545, United States;*

orcid.org/0000-0001-9679-6020; Email: gaunt@lanl.gov

Nikolas Kaltsoyannis − *Centre for Radiochemistry Research, The University of Manchester, Oxford Road, Manchester M13 9PL, U.K.; Department of Chemistry, The University of Manchester, Oxford Road, Manchester M13 9PL, U.K.;* orcid.org/0000-0003-0293-5742; Email: nikolas.kaltsoyannis@manchester.ac.uk

Authors

Conrad A. P. Goodwin − *Chemistry Division, Los Alamos National Laboratory, Los Alamos, New Mexico 87545, United States; Centre for Radiochemistry Research, The University of Manchester, Oxford Road, Manchester M13 9PL, U.K.; Department of Chemistry, The University of Manchester, Oxford Road, Manchester M13 9PL, U.K.;* orcid.org/0000-0002-4320-2548

Ralph W. Adams − *Department of Chemistry, The University of Manchester, Oxford Road, Manchester M13 9PL, U.K.;* orcid.org/0000-0001-8009-5334

Susan K. Hanson − *Chemistry Division, Los Alamos National Laboratory, Los Alamos, New Mexico 87545, United States;* orcid.org/0000-0002-3230-8400

Michael T. Janicke − *Chemistry Division, Los Alamos National Laboratory, Los Alamos, New Mexico 87545, United States*

Stephen T. Liddle − *Centre for Radiochemistry Research, The University of Manchester, Oxford Road, Manchester M13 9PL, U.K.; Department of Chemistry, The University of Manchester, Oxford Road, Manchester M13 9PL, U.K.;* orcid.org/0000-0001-9911-8778

Iain May − *Chemistry Division, Los Alamos National Laboratory, Los Alamos, New Mexico 87545, United States*

Jeffrey L. Miller − *Chemistry Division, Los Alamos National Laboratory, Los Alamos, New Mexico 87545, United States*

Brian L. Scott − *Materials Physics & Applications Division, Los Alamos National Laboratory, Los Alamos, New Mexic 87545, United States*

John A. Seed − *Centre for Radiochemistry Research, The University of Manchester, Oxford Road, Manchester M13 9PL, U.K.; Department of Chemistry, The University of Manchester, Oxford Road, Manchester M13 9PL, U.K.;* orcid.org/0000-0002-3751-0325

George F. S. Whitehead − *Department of Chemistry, The University of Manchester, Oxford Road, Manchester M13 9PL, U.K.;* orcid.org/0000-0003-1949-4250

Complete contact information is available at: https://pubs.acs.org/10.1021/jacs.3c12721

Notes

The authors declare no competing financial interest.

■ ACKNOWLEDGMENTS

Experimental work (except for VT-NMR measurements on **2La**) was conducted at the Los Alamos National Laboratory (LANL) for which C.A.P.G., A.J.G., and B.L.S. thank the U.S. Department of Energy, Office of Science, Office of Basic Energy Sciences, Chemical Sciences, Geosciences, and Biosciences Division, Heavy Element Chemistry Program at LANL (contract DE-AC52-06NA25396). C.A.P.G. also thanks the LANL Laboratory Directed Research and Development (LDRD) program for a Distinguished J. R. Oppenheimer Postdoctoral Fellowship (LANL-LDRD 20180703PRD1) and the Royal Society for a University Research Fellowship (URF \211271) during manuscript preparation, data analysis, and supporting synthetic work. For computational work, N.K. is grateful to the University of Manchester for computing resources via its Computational Shared Facility and associated support services. S.T.L. thanks the Alexander von Humboldt Foundation for a Freidrich Wilhelm Bessel Research Award and the EPSRC (EP/M027015/1). We acknowledge funding from the EPSRC (EP/V007580/1 and EP/K039547/1) for NMR spectroscopy resources. Research data files supporting a portion of this publication are available from Figshare at doi: 10.48420/25037141.

■ REFERENCES

(1) Clark, D. L.; Geeson, D. A.; Hanrahan, R. J., Jr. *Plutonium Handbook*; American Nuclear Society, 2019.

(2) Cotton, S. *Lanthanide and Actinide Chemistry*; John Wiley & Sons, Ltd, 2006.

(3) Liddle, S. T.; Mills, D. P.; Natrajan, L. S. The Lanthanides and Actinides: Synthesis, Reactivity, Properties and Applications. *Lanthanides and Actinides*; Chemistry LibreTexts, 2022.

(4) Morss, L. R.; Edelstein, N. M.; Fuger, J. *The Chemistry of the Actinide and Transactinide Elements*; Springer Dordrecht, 2011.

(5) Birnbaum, E. R.; Fassbender, M. E.; Ferrier, M. G.; John, K. D.; Mastren, T. Actinides in Medicine. In *Encyclopedia of Inorganic and Bioinorganic Chemistry*; Scott, R. A., Ed.; Wiley Online Library, 2020; pp 1−21.

(6) Liddle, S. T. The Renaissance of Non-Aqueous Uranium Chemistry. *Angew. Chem., Int. Ed.* **2015**, *54* (30), 8604−8641.

(7) Hayton, T. W. Metal-ligand multiple bonding in uranium: structure and reactivity. *Dalton Trans.* **2010**, *39* (5), 1145−1158.

(8) Kelley, M. P.; Su, J.; Urban, M.; Luckey, M.; Batista, E. R.; Yang, P.; Shafer, J. C. On the Origin of Covalent Bonding in Heavy Actinides. *J. Am. Chem. Soc.* **2017**, *139* (29), 9901−9908.

(9) Kaltsoyannis, N. Transuranic Computational Chemistry. *Chem.—Eur. J.* **2018**, *24* (12), 2815−2825.

(10) Kaltsoyannis, N. Does covalency increase or decrease across the actinide series? Implications for minor actinide partitioning. *Inorg. Chem.* **2013**, *52* (7), 3407−3413.

(11) Jones, M. B.; Gaunt, A. J.; Gordon, J. C.; Kaltsoyannis, N.; Neu, M. P.; Scott, B. L. Uncovering f-element bonding differences and electronic structure in a series of 1:3 and 1:4 complexes with a diselenophosphinate ligand. *Chem. Sci.* **2013**, *4* (3), 1189−1203.

(12) Kirker, I.; Kaltsoyannis, N. Does covalency *really* increase across the 5f series? A comparison of molecular orbital, natural population, spin and electron density analyses of $AnCp_3$ (An = Th-Cm; Cp = η^5-C_5H_5). *Dalton Trans.* **2011**, *40* (1), 124−131.

(13) Tassell, M. J.; Kaltsoyannis, N. Covalency in $AnCp_4$ (An = Th-Cm): a comparison of molecular orbital, natural population and atoms-in-molecules analyses. *Dalton Trans.* **2010**, *39* (29), 6719−6725.

(14) Goodwin, C. A. P.; Schlimgen, A. W.; Albrecht-Schönzart, T. E.; Batista, E. R.; Gaunt, A.; Janicke, M. T.; Kozimor, S. A.; Scott, B. L.; Stevens, L. M.; White, F. D.; Yang, P. Structural and spectroscopic comparison of soft-Se vs hard-O donor bonding in trivalent americium/neodymium molecules. *Angew. Chem., Int. Ed.* **2021**, *60* (17), 9459−9466.

(15) Ingram, K. I.; Tassell, M. J.; Gaunt, A. J.; Kaltsoyannis, N. Covalency in the f Element-Chalcogen Bond. Computational Studies of $M[N(EPR_2)_2]_3$ (M = La, Ce, Pr, Pm, Eu, U, Np, Pu, Am, Cm; E = O, S, Se, Te; R = H, ^{i}Pr, Ph). *Inorg. Chem.* **2008**, *47* (17), 7824−7833.

(16) Gaunt, A. J.; Reilly, S. D.; Enriquez, A. E.; Scott, B. L.; Ibers, J. A.; Sekar, P.; Ingram, K. I.; Kaltsoyannis, N.; Neu, M. P. Experimental and theoretical comparison of actinide and lanthanide bonding in $M[N(EPR_2)_2]_3$ complexes (M = U, Pu, La, Ce; E = S, Se, Te; R = Ph, *i*Pr, H). *Inorg. Chem.* **2008**, *47* (1), 29−41.

(17) Gaunt, A. J.; Scott, B. L.; Neu, M. P. A Molecular Actinide-Tellurium Bond and Comparison of Bonding in $[M^{III}\{N$-

$(\mathrm{TeP}i\mathrm{Pr}_2)_2\}_3]$ (M = U, La). *Angew. Chem., Int. Ed.* **2006**, *45* (10), 1638−1641.

(18) Long, B. N.; Beltrán-Leiva, M. J.; Celis-Barros, C.; Sperling, J. M.; Poe, T. N.; Baumbach, R. E.; Windorff, C. J.; Albrecht-Schönzart, T. E. Cyclopentadienyl coordination induces unexpected ionic Am-N bonding in an americium bipyridyl complex. *Nat. Commun.* **2022**, *13* (1), 201.

(19) Sperling, J. M.; Warzecha, E. J.; Celis-Barros, C.; Sergentu, D. C.; Wang, X.; Klamm, B. E.; Windorff, C. J.; Gaiser, A. N.; White, F. D.; Beery, D. A.; Chemey, A. T.; Whitefoot, M. A.; Long, B. N.; Hanson, K.; Kogerler, P.; Speldrich, M.; Zurek, E.; Autschbach, J.; Albrecht-Schönzart, T. E. Compression of curium pyrrolidine-dithiocarbamate enhances covalency. *Nature* **2020**, *583* (7816), 396−399.

(20) Greer, R. D. M.; Celis-Barros, C.; Sperling, J. M.; Gaiser, A. N.; Windorff, C. J.; Albrecht-Schönzart, T. E. Structure and Characterization of an Americium Bis(*O*, *O*'-diethyl)dithiophosphate Complex. *Inorg. Chem.* **2020**, *59* (22), 16291−16300.

(21) Denning, R. G.; Snellgrove, T. R.; Woodwark, D. R. The electronic structure of the uranyl ion. *Mol. Phys.* **1979**, *37* (4), 1109−1143.

(22) Denning, R. G.; Green, J. C.; Hutchings, T. E.; Dallera, C.; Tagliaferri, A.; Giarda, K.; Brookes, N. B.; Braicovich, L. Covalency in the uranyl ion: A polarized x-ray spectroscopic study. *J. Chem. Phys.* **2002**, *117* (17), 8008−8020.

(23) Hayton, T. W.; Boncella, J. M.; Scott, B. L.; Palmer, P. D.; Batista, E. R.; Hay, P. J. Synthesis of imido analogs of the uranyl ion. *Science* **2005**, *310* (5756), 1941−1943.

(24) Anderson, N. H.; Odoh, S. O.; Yao, Y.; Williams, U. J.; Schaefer, B. A.; Kiernicki, J. J.; Lewis, A. J.; Goshert, M. D.; Fanwick, P. E.; Schelter, E. J.; Walensky, J. R.; Gagliardi, L.; Bart, S. C. Harnessing redox activity for the formation of uranium tris(imido) compounds. *Nat. Chem.* **2014**, *6* (10), 919−926.

(25) Goodwin, C. A. P.; Wooles, A. J.; Murillo, J.; Lu, E.; Boronski, J. T.; Scott, B. L.; Gaunt, A. J.; Liddle, S. T. Carbene Complexes of Neptunium. *J. Am. Chem. Soc.* **2022**, *144* (22), 9764−9774.

(26) Dutkiewicz, M. S.; Goodwin, C. A. P.; Perfetti, M.; Gaunt, A. J.; Griveau, J.-C.; Colineau, E.; Kovács, A.; Wooles, A. J.; Caciuffo, R.; Walter, O.; Liddle, S. T. A Terminal Neptunium(V)-Mono(Oxo) Complex. *Nat. Chem.* **2022**, *14*, 342−349.

(27) Wooles, A. J.; Mills, D. P.; Tuna, F.; McInnes, E. J. L.; Law, G. T. W.; Fuller, A. J.; Kremer, F.; Ridgway, M.; Lewis, W.; Gagliardi, L.; Vlaisavljevich, B.; Liddle, S. T. Uranium(III)-carbon multiple bonding supported by arene δ-bonding in mixed-valence hexauranium nanometre-scale rings. *Nat. Commun.* **2018**, *9* (1), 2097.

(28) Kent, G. T.; Yu, X.; Wu, G.; Autschbach, J.; Hayton, T. W. Synthesis and electronic structure analysis of the actinide allenylidenes, $[\{(\mathrm{NR}_2)_3\}\mathrm{An}(\mathrm{CCCPh}_2)]^{--}$ (An = U, Th; R = SiMe_3). *Chem. Sci.* **2021**, *12* (43), 14383−14388.

(29) Staun, S. L.; Sergentu, D. C.; Wu, G.; Autschbach, J.; Hayton, T. W. Use of ^{15}N NMR spectroscopy to probe covalency in a thorium nitride. *Chem. Sci.* **2019**, *10* (26), 6431−6436.

(30) Smiles, D. E.; Wu, G.; Hrobárik, P.; Hayton, T. W. Use of ^{77}Se and ^{125}Te NMR Spectroscopy to Probe Covalency of the Actinide-Chalcogen Bonding in $[\mathrm{Th}(\mathrm{E_n})\{\mathrm{N}(\mathrm{SiMe}_3)_2\}_3]^{--}$ (E = Se, Te; n = 1, 2) and Their Oxo-Uranium(VI) Congeners. *J. Am. Chem. Soc.* **2016**, *138* (3), 814−825.

(31) Mullane, K. C.; Hrobarik, P.; Cheisson, T.; Manor, B. C.; Carroll, P. J.; Schelter, E. J. ^{13}C NMR Shifts as an Indicator of U-C Bond Covalency in Uranium(VI) Acetylide Complexes: An Experimental and Computational Study. *Inorg. Chem.* **2019**, *58* (7), 4152−4163.

(32) Cheisson, T.; Kersey, K. D.; Mahieu, N.; McSkimming, A.; Gau, M. R.; Carroll, P. J.; Schelter, E. J. Multiple Bonding in Lanthanides and Actinides: Direct Comparison of Covalency in Thorium(IV)- and Cerium(IV)-Imido Complexes. *J. Am. Chem. Soc.* **2019**, *141* (23), 9185−9190.

(33) Lu, E.; Boronski, J. T.; Gregson, M.; Wooles, A. J.; Liddle, S. T. Silyl-Phosphino-Carbene Complexes of Uranium(IV). *Angew. Chem., Int. Ed.* **2018**, *57* (19), 5506−5511.

(34) Du, J.; Seed, J. A.; Berryman, V. E. J.; Kaltsoyannis, N.; Adams, R. W.; Lee, D.; Liddle, S. T. Exceptional uranium(VI)-nitride triple bond covalency from ^{15}N nuclear magnetic resonance spectroscopy and quantum chemical analysis. *Nat. Commun.* **2021**, *12* (1), 5649.

(35) Adam, C.; Kaden, P.; Beele, B. B.; Müllich, U.; Trumm, S.; Geist, A.; Panak, P. J.; Denecke, M. A. Evidence for covalence in a N-donor complex of americium(III). *Dalton Trans.* **2013**, *42* (39), 14068−14074.

(36) Law, J. D.; Peterman, D. R.; Todd, T. A.; Tillotson, R. D. Separation of trivalent actinides from lanthanides in an acetate buffer solution using Cyanex 301. *Radiochim. Acta* **2006**, *94* (5), 261−266.

(37) Chen, J.; Wang, S.; Xu, C.; Wang, X.; Feng, X. Separation of Americium from Lanthanides by Purified Cyanex 301 Countercurrent Extraction in Miniature Centrifugal Contactors. *Procedia Chem.* **2012**, *7*, 172−177.

(38) Panak, P. J.; Geist, A. Complexation and Extraction of Trivalent Actinides and Lanthanides by Triazinylpyridine N-Donor Ligands. *Chem. Rev.* **2013**, *113* (2), 1199−1236.

(39) Lewis, F. W.; Harwood, L. M.; Hudson, M. J.; Drew, M. G. B.; Desreux, J. F.; Vidick, G.; Bouslimani, N.; Modolo, G.; Wilden, A.; Sypula, M.; Vu, T.-H.; Simonin, J.-P. Highly Efficient Separation of Actinides from Lanthanides by a Phenanthroline-Derived Bis-triazine Ligand. *J. Am. Chem. Soc.* **2011**, *133* (33), 13093−13102.

(40) Nilsson, M.; Nash, K. L. Review Article: A Review of the Development and Operational Characteristics of the TALSPEAK Process. *Solvent Extr. Ion Exch.* **2007**, *25* (6), 665−701.

(41) Gelis, A. V.; Lumetta, G. J. Actinide Lanthanide Separation Process—ALSEP. *Ind. Eng. Chem. Res.* **2014**, *53* (4), 1624−1631.

(42) Gilson, S. E.; Burns, P. C. The crystal and coordination chemistry of neptunium in all its oxidation states: An expanded structural hierarchy of neptunium compounds. *Coord. Chem. Rev.* **2021**, *445*, 213994.

(43) Gaunt, A. J.; Scott, B. L.; Neu, M. P. Homoleptic uranium(III) imidodiphosphinochalcogenides including the first structurally characterised molecular trivalent actinide-Se bond. *Chem. Commun.* **2005**, 3215−3217.

(44) Ingram, K. I. M.; Kaltsoyannis, N.; Gaunt, A. J.; Neu, M. P. Covalency in the f-element-chalcogen bond: Computational studies of $[\mathrm{M}(\mathrm{N}(\mathrm{EPH}_2)_2)_3]$ (M = La, U, Pu; E = O, S, Se, Te). *J. Alloys Compd.* **2007**, *444−445*, 369−375.

(45) Macor, J. A.; Brown, J. L.; Cross, J. N.; Daly, S. R.; Gaunt, A. J.; Girolami, G. S.; Janicke, M. T.; Kozimor, S. A.; Neu, M. P.; Olson, A. C.; Reilly, S. D.; Scott, B. L. Coordination chemistry of 2,2'-biphenylenedithiophosphinate and diphenyldithiophosphinate with U, Np, and Pu. *Dalton Trans.* **2015**, *44* (43), 18923−18936.

(46) Cary, S. K.; Su, J.; Galley, S. S.; Albrecht-Schmitt, T. E.; Batista, E. R.; Ferrier, M. G.; Kozimor, S. A.; Mocko, V.; Scott, B. L.; Van Alstine, C. E.; White, F. D.; Yang, P. A series of dithiocarbamates for americium, curium, and californium. *Dalton Trans.* **2018**, *47* (41), 14452−14461.

(47) Long, B. N.; Sperling, J. M.; Windorff, C. J.; Huffman, Z. K.; Albrecht-Schonzart, T. E. Expanding Transuranium Organoactinide Chemistry: Synthesis and Characterization of $(\mathrm{Cp'}_3\mathrm{M})_2(\mu\text{-}4,4'\text{-bpy})$ (M = Ce, Np, Pu). *Inorg. Chem.* **2023**, *62* (16), 6368−6374.

(48) Clegg, W.; Blake, A. J.; Cole, J. M.; Evans, J. S. O.; Main, P.; Parsons, S.; Watkin, D. J. *Crystal Structure Analysis*; Oxford University Press, 2009.

(49) Neidig, M. L.; Clark, D. L.; Martin, R. L. Covalency in f-element complexes. *Coord. Chem. Rev.* **2013**, *257* (2), 394−406.

(50) Kovacs, A.; Apostolidis, C.; Walter, O. Competing Metal-Ligand Interactions in Tris(cyclopentadienyl)-cyclohexylisonitrile Complexes of Trivalent Actinides and Lanthanides. *Molecules* **2022**, *27* (12), 3811.

(51) Mehdoui, T.; Berthet, J. C.; Thuéry, P.; Ephritikhine, M. The remarkable efficiency of N-heterocyclic carbenes in lanthanide(III)/actinide(III) differentiation. *Chem. Commun.* **2005**, 2860−2862.

(52) del Mar Conejo, M.; Parry, J. S.; Carmona, E.; Schultz, M.; Brennann, J. G.; Beshouri, S. M.; Andersen, R. A.; Rogers, R. D.; Coles, S.; Hursthouse, M. Carbon Monoxide and Isocyanide Complexes of Trivalent Uranium Metallocenes. *Chem.—Eur. J.* **1999**, *5* (10), 3000−3009.

(53) Evans, W. J.; Kozimor, S. A.; Ziller, J. W. A monometallic f element complex of dinitrogen: $(C_5Me_5)_3U(\eta^1\text{-}N_2)$. *J. Am. Chem. Soc.* **2003**, *125* (47), 14264−14265.

(54) Evans, W. J.; Kozimor, S. A.; Nyce, G. W.; Ziller, J. W. Comparative reactivity of sterically crowded nf^3 $(C_5Me_5)_3Nd$ and $(C_5Me_5)_3U$ complexes with CO: formation of a nonclassical carbonium ion versus an f element metal carbonyl complex. *J. Am. Chem. Soc.* **2003**, *125* (45), 13831−13835.

(55) Lukens, W. W.; Speldrich, M.; Yang, P.; Duignan, T. J.; Autschbach, J.; Kögerler, P. The roles of 4f- and 5f-orbitals in bonding: a magnetochemical, crystal field, density functional theory, and multi-reference wavefunction study. *Dalton Trans.* **2016**, *45* (28), 11508−11521.

(56) Nakai, H.; Hu, X.; Zakharov, L. N.; Rheingold, A. L.; Meyer, K. Synthesis and characterization of N-heterocyclic carbene complexes of uranium(III). *Inorg. Chem.* **2004**, *43* (3), 855−857.

(57) Maron, L.; Eisenstein, O.; Andersen, R. A. The Bond between CO and Cp'_3U in $Cp'_3U(CO)$ Involves Back-bonding from the Cp'_3U Ligand-Based Orbitals of π-Symmetry, where Cp′ Represents a Substituted Cyclopentadienyl Ligand. *Organometallics* **2009**, *28* (13), 3629−3635.

(58) Mehdoui, T.; Berthet, J. C.; Thuéry, P.; Ephritikhine, M. Clear-Cut Lanthanide(III)/Actinide(III) Differentiation in Coordination of Pyrazine to Tris(cyclopentadienyl) Complexes of Cerium and Uranium, Involving Reversible $U^{III}\rightarrow U^{IV}$ Oxidation. *Eur. J. Inorg. Chem.* **2004**, *2004* (10), 1996−2000.

(59) Brennan, J. G.; Stults, S. D.; Andersen, R. A.; Zalkin, A. Crystal structures of $(MeC_5H_4)_3ML$ [M = uranium or cerium; L = quinuclidine or $P(OCH_2)_3CEt$]. Evidence for uranium to phosphorus π-back-bonding. *Organometallics* **1988**, *7* (6), 1329−1334.

(60) Berthet, J.-C.; Miquel, Y.; Iveson, P. B.; Nierlich, M.; Thuéry, P.; Madic, C.; Ephritikhine, M. The affinity and selectivity of terdentate nitrogen ligands towards trivalent lanthanide and uranium ions viewed from the crystal structures of the 1−3 complexes. *J. Chem. Soc., Dalton Trans.* **2002**, No. 16, 3265−3272.

(61) Seed, J. A.; Gregson, M.; Tuna, F.; Chilton, N. F.; Wooles, A. J.; McInnes, E. J. L.; Liddle, S. T. Rare-Earth- and Uranium-Mesoionic Carbenes: A New Class of f-Block Carbene Complex Derived from an N-Heterocyclic Olefin. *Angew. Chem., Int. Ed.* **2017**, *56* (38), 11534−11538.

(62) Shephard, J. J.; Berryman, V. E. J.; Ochiai, T.; Walter, O.; Price, A. N.; Warren, M. R.; Arnold, P. L.; Kaltsoyannis, N.; Parsons, S. Covalent bond shortening and distortion induced by pressurization of thorium, uranium, and neptunium tetrakis aryloxides. *Nat. Commun.* **2022**, *13* (1), 5923.

(63) Goodwin, C. A. P.; Tuna, F.; McInnes, E. J. L.; Liddle, S. T.; McMaster, J.; Vitorica-Yrezabal, I. J.; Mills, D. P. $[U^{III}\{N(SiMe_2tBu)_2\}_3]$: a structurally authenticated trigonal planar actinide complex. *Chem.—Eur. J.* **2014**, *20* (45), 14579−14583.

(64) Cross, J. N.; Su, J.; Batista, E. R.; Cary, S. K.; Evans, W. J.; Kozimor, S. A.; Mocko, V.; Scott, B. L.; Stein, B. W.; Windorff, C. J.; Yang, P. Covalency in Americium(III) Hexachloride. *J. Am. Chem. Soc.* **2017**, *139* (25), 8667−8677.

(65) Galley, S. S.; Sperling, J. M.; Windorff, C. J.; Zeller, M.; Albrecht-Schmitt, T. E.; Bart, S. C. Conversion of Americia to Anhydrous Trivalent Americium Halides. *Organometallics* **2019**, *38* (3), 606−609.

(66) Wedal, J. C.; Windorff, C. J.; Huh, D. N.; Ryan, A. J.; Ziller, J. W.; Evans, W. J. Structural variations in cyclopentadienyl uranium(III) iodide complexes. *J. Coord. Chem.* **2021**, *74* (1−3), 74−91.

(67) Windorff, C. J.; Sperling, J. M.; Albrecht-Schönzart, T. E.; Bai, Z.; Evans, W. J.; Gaiser, A. N.; Gaunt, A. J.; Goodwin, C. A. P.; Hobart, D. E.; Huffman, Z. K.; Huh, D. N.; Klamm, B. E.; Poe, T. N.; Warzecha, E. A Single Small-Scale Plutonium Redox Reaction System Yields Three Crystallographically-Characterizable Organoplutonium Complexes. *Inorg. Chem.* **2020**, *59* (18), 13301−13314.

(68) Goodwin, C. A. P.; Janicke, M. T.; Scott, B. L.; Gaunt, A. J. $[AnI_3(THF)_4]$ (An = Np, Pu) preparation bypassing An^0 metal precursors: access to Np^{3+}/Pu^{3+} nonaqueous and organometallic complexes. *J. Am. Chem. Soc.* **2021**, *143* (49), 20680−20696.

(69) Černá, M.; Seed, J. A.; Garrido-Fernandez, S.; Janicke, M. T.; Scott, B. L.; Whitehead, G. F. S.; Gaunt, A. J.; Goodwin, C. A. P. Isostructural σ-hydrocarbyl phospholide complexes of uranium, neptunium, and plutonium. *Chem. Commun.* **2022**, *58* (95), 13278−13281.

(70) Goodwin, C. A. P.; Ciccone, S. R.; Bekoe, S.; Majumdar, S.; Scott, B. L.; Ziller, J. W.; Gaunt, A. J.; Furche, F.; Evans, W. J. 2.2.2-Cryptand complexes of neptunium(III) and plutonium(III). *Chem. Commun.* **2022**, *58* (7), 997−1000.

(71) Long, B. N.; Beltran-Leiva, M. J.; Sperling, J. M.; Poe, T. N.; Celis-Barros, C.; Albrecht-Schonzart, T. E. Altering the spectroscopy, electronic structure, and bonding of organometallic curium(III) upon coordination of 4,4′-bipyridine. *Nat. Commun.* **2023**, *14* (1), 3774.

(72) Arnold, P. L.; Casely, I. J. F-block N-heterocyclic carbene complexes. *Chem. Rev.* **2009**, *109* (8), 3599−3611.

(73) Hopkinson, M. N.; Richter, C.; Schedler, M.; Glorius, F. An overview of N-heterocyclic carbenes. *Nature* **2014**, *510* (7506), 485−496.

(74) Bourissou, D.; Guerret, O.; Gabbaï, F. P.; Bertrand, G. Stable Carbenes. *Chem. Rev.* **2000**, *100* (1), 39−92.

(75) Nelson, D. J.; Nolan, S. P. Quantifying and understanding the electronic properties of N-heterocyclic carbenes. *Chem. Soc. Rev.* **2013**, *42* (16), 6723−6753.

(76) Huynh, H. V. Electronic Properties of N-Heterocyclic Carbenes and Their Experimental Determination. *Chem. Rev.* **2018**, *118* (19), 9457−9492.

(77) Huynh, H. V.; Frison, G. Electronic structural trends in divalent carbon compounds. *J. Org. Chem.* **2013**, *78* (2), 328−338.

(78) Jacobsen, H.; Correa, A.; Costabile, C.; Cavallo, L. π-Acidity and π-basicity of N-heterocyclic carbene ligands. A computational assessment. *J. Organomet. Chem.* **2006**, *691* (21), 4350−4358.

(79) Scott, N. M.; Dorta, R.; Stevens, E. D.; Correa, A.; Cavallo, L.; Nolan, S. P. Interaction of a bulky *N*-heterocyclic carbene ligand with Rh(I) and Ir(I). Double C-H activation and isolation of bare 14-electron Rh(III) and Ir(III) complexes. *J. Am. Chem. Soc.* **2005**, *127* (10), 3516−3526.

(80) Maron, L.; Bourissou, D. Lanthanide Complexes of Amino-Carbenes: On the Samarium-Carbene Bond from DFT Calculations. *Organometallics* **2007**, *26* (4), 1100−1103.

(81) Goodwin, C. A. P.; Su, J.; Albrecht-Schmitt, T. E.; Blake, A. V.; Batista, E. R.; Daly, S. R.; Dehnen, S.; Evans, W. J.; Gaunt, A. J.; Kozimor, S. A.; Lichtenberger, N.; Scott, B. L.; Yang, P. $[Am(C_5Me_4H)_3]$: An Organometallic Americium Complex. *Angew. Chem., Int. Ed.* **2019**, *58* (34), 11695−11699.

(82) Evans, W. J.; Grate, J. W.; Levan, K. R.; Bloom, I.; Peterson, T. T.; Doedens, R. J.; Zhang, H.; Atwood, J. L. Synthesis and x-ray crystal structure of di(pentamethylcyclopentadienyl)lanthanide and yttrium halide complexes. *Inorg. Chem.* **1986**, *25* (20), 3614−3619.

(83) Meng, Y. S.; Zhang, Y. Q.; Wang, Z. M.; Wang, B. W.; Gao, S. Weak Ligand-Field Effect from Ancillary Ligands on Enhancing Single-Ion Magnet Performance. *Chem.—Eur. J.* **2016**, *22* (36), 12724−12731.

(84) CCDC 125077.

(85) Zwick, B. D.; Sattelberger, A. P.; Avens, L. R. Transuranium Organometallics Elements: The Next Generation. In *Transuranium Elements: A Half Century*; Morss, L. R., Fuger, J., Eds.; American Chemical Society, 1992; pp 239−246.

(86) Grimme, S.; Antony, J.; Ehrlich, S.; Krieg, H. A consistent and accurate ab initio parametrization of density functional dispersion correction (DFT-D) for the 94 elements H-Pu. *J. Chem. Phys.* **2010**, *132* (15), 154104.

(87) Su, J.; Batista, E. R.; Boland, K. S.; Bone, S. E.; Bradley, J. A.; Cary, S. K.; Clark, D. L.; Conradson, S. D.; Ditter, A. S.; Kaltsoyannis,

N.; Keith, J. M.; Kerridge, A.; Kozimor, S. A.; Loble, M. W.; Martin, R. L.; Minasian, S. G.; Mocko, V.; La Pierre, H. S.; Seidler, G. T.; Shuh, D. K.; Wilkerson, M. P.; Wolfsberg, L. E.; Yang, P. Energy-Degeneracy-Driven Covalency in Actinide Bonding. *J. Am. Chem. Soc.* **2018**, *140* (51), 17977−17984.

(88) Cross, J. N.; Macor, J. A.; Bertke, J. A.; Ferrier, M. G.; Girolami, G. S.; Kozimor, S. A.; Maassen, J. R.; Scott, B. L.; Shuh, D. K.; Stein, B. W.; Stieber, S. C. Comparing the 2,2′-Biphenylenedithiophosphinate Binding of Americium with Neodymium and Europium. *Angew. Chem., Int. Ed.* **2016**, *55* (41), 12755−12759.

(89) Windorff, C. J.; Celis-Barros, C.; Sperling, J. M.; McKinnon, N. C.; Albrecht-Schmitt, T. E. Probing a variation of the inverse-trans-influence in americium and lanthanide tribromide tris(tricyclohexylphosphine oxide) complexes. *Chem. Sci.* **2020**, *11* (10), 2770−2782.

(90) Jensen, M. P.; Bond, A. H. Comparison of Covalency in the Complexes of Trivalent Actinide and Lanthanide Cations. *J. Am. Chem. Soc.* **2002**, *124* (33), 9870−9877.

(91) Shannon, R. D. Revised effective ionic radii and systematic studies of interatomic distances in halides and chalcogenides. *Acta Crystallogr., Sect. A: Cryst. Phys., Diffr., Theor. Gen. Crystallogr.* **1976**, *32* (5), 751−767.

(92) Crabtree, R. H. *The Organometallic Chemistry of the Transition Metals*; John Wiley & Sons, Inc., 2014.

(93) Bursten, B. E.; Rhodes, L. F.; Strittmatter, R. J. The bonding in tris(η^5-cyclopentadienyl) actinide complexes IV: Electronic structural effects in $AnCl_3$ and $(\eta^5\text{-}C_5H_5)_3An$ (An ≡ Th - Cf) complexes. *J. Less-Common Met.* **1989**, *149*, 207−211.

(94) Bursten, B. E.; Rhodes, L. F.; Strittmatter, R. J. Bonding of tris(η^5-cyclopentadienyl) actinide complexes. 3. Interaction of π-neutral, π-acidic, and π-basic ligands with $(\eta^5\text{-}C_5H_5)_3U$. *J. Am. Chem. Soc.* **1989**, *111* (8), 2758−2766.

(95) Bursten, B. E.; Rhodes, L. F.; Strittmatter, R. J. Bonding in tris(η^5-cyclopentadienyl) actinide complexes. 2. The ground electronic configurations of ″base-free″ Cp_3An complexes (An = thorium, protactinium, uranium, neptunium, plutonium). *J. Am. Chem. Soc.* **1989**, *111* (8), 2756−2758.

(96) Strittmatter, R. J.; Bursten, B. E. Bonding in tris(η^5-cyclopentadienyl) actinide complexes. 5. A comparison of the bonding in neptunium, plutonium, and transplutonium compounds with that in lanthanide compounds and a transition-metal analog. *J. Am. Chem. Soc.* **1991**, *113* (2), 552−559.

(97) Bursten, B. E.; Palmer, E. J.; Sonnenberg, J. L. On the Role of *f*-Orbitals in the Bonding in *f*-Element Complexes: the "Feudal" Model as Applied to Organoactinide and Actinide Aquo Complexes. In *Recent Advances In Actinide Science*; Alvares, R., Bryan, N. D., May, I., Eds.; Special Publications, The Royal Society of Chemistry, 2006; pp 157−162.

(98) Murillo, J.; Seed, J. A.; Wooles, A. J.; Oakley, M. S.; Goodwin, C. A. P.; Gregson, M.; Dan, D.; Chilton, N. F.; Gaunt, A. J.; Kozimor, S. A.; Liddle, S. T.; Scott, B. L. Carbene Complexes of Plutonium: Structure, Bonding, and Divergent Reactivity to Lanthanide Analogs. *J. Am. Chem. Soc.* **2024**, *146* (6), 4098−4111.

(99) Hargreaves, W. A. Energy levels of Pr^{3+} ions in halide crystals. *J. Condens Matter. Phys.* **1992**, *4* (28), 6141−6154.

(100) Carnall, W. T.; Fields, P. R.; Rajnak, K. Electronic Energy Levels in the Trivalent Lanthanide Aquo Ions. I. Pr^{3+}, Nd^{3+}, Pm^{3+}, Sm^{3+}, Dy^{3+}, Ho^{3+}, Er^{3+}, and Tm^{3+}. *J. Chem. Phys.* **1968**, *49* (10), 4424−4442.

(101) Sugar, J. Energy Levels of Pr^{3+} in the Vapor State. *Phys. Rev. Lett.* **1965**, *14* (18), 731−732.

(102) Sarup, R.; Crozier, M. H. Analysis of the Eigenstates of Pr^{3+} in $LaCl_3$ Using the Zeeman Effect in High Fields. *J. Chem. Phys.* **1965**, *42* (1), 371−376.

(103) Crosswhite, H. M.; Dieke, G. H.; Carter, W. J. Free-Ion and Crystalline Spectra of Pr^{3+} (Pr IV). *J. Chem. Phys.* **1965**, *43* (6), 2047−2054.

(104) Caspers, H. H.; Rast, H. E.; Buchanan, R. A. Energy Levels of Pr^{3+} in LaF_3. *J. Chem. Phys.* **1965**, *43* (6), 2124−2128.

(105) Carnall, W. T.; Fields, P. R.; Wybourne, B. G. Spectral Intensities of the Trivalent Lanthanides and Actinides in Solution. I. Pr^{3+}, Nd^{3+}, Er^{3+}, Tm^{3+}, and Yb^{3+}. *J. Chem. Phys.* **1965**, *42* (11), 3797−3806.

(106) Carnall, W. T.; Fields, P. R. Lanthanide and Actinide Absorption Spectra in Solution. *Lanthanide/Actinide Chemistry*; Advances in Chemistry; American Chemical Society, 1967; Vol. *71*, pp 86−101.

(107) Carnall, W. T. A systematic analysis of the spectra of trivalent actinide chlorides in D_{3h} site symmetry. *J. Chem. Phys.* **1992**, *96* (12), 8713−8726.

(108) Carnall, W. T.; Wybourne, B. G. Electronic Energy Levels of the Lighter Actinides: U^{3+}, Np^{3+}, Pu^{3+}, Am^{3+}, and Cm^{3+}. *J. Chem. Phys.* **1964**, *40* (11), 3428−3433.

(109) Carnall, W. T.; Crosswhite, H.; Crosswhite, H. M.; Hessler, J. P.; Edelstein, N.; Conway, J. G.; Shalimoff, G. V.; Sarup, R. Energy level analysis of Np^{3+}:$LaCl_3$ and Np^{3+}:$LaBr_3$. *J. Chem. Phys.* **1980**, *72* (9), 5089−5102.

(110) Varga, L. P.; Baybarz, R. D.; Reisfeld, M. J.; Asprey, L. B. Electronic spectra of the $5f^5$ and $5f^9$ actinides: Am^{4+}, Pu^{3+}, Bk^{2+}, Cf^{3+} and Es^{4+}. *J. Inorg. Nucl. Chem.* **1973**, *35* (8), 2775−2785.

(111) Goodwin, C. A. P.; Su, J.; Stevens, L. M.; White, F. D.; Anderson, N. H.; Auxier, J. D.; Albrecht-Schönzart, T. E.; Batista, E. R.; Briscoe, S. F.; Cross, J. N.; Evans, W. J.; Gaiser, A. N.; Gaunt, A. J.; James, M. R.; Janicke, M. T.; Jenkins, T. F.; Jones, Z. R.; Kozimor, S. A.; Scott, B. L.; Sperling, J. M.; Wedal, J. C.; Windorff, C. J.; Yang, P.; Ziller, J. W. Isolation and Characterization of a Californium Metallocene. *Nature* **2021**, *599* (7885), 421−424.